CHAPTER 4

DELIVERY OF SEDIMENT TO BASINS BY FLUVIAL SYSTEMS

In this chapter we discuss streams and rivers, the most fundamental agents of landscape evolution and sediment delivery to basins. Engineers refer to the running water of streams and rivers as open channel flow, in contrast to pipe flows. Open channel flows may be unsteady in time, or nonuniform in space, or both. They may be three dimensional, with significant cross-channel and vertical components, and may show abrupt increases in discharge as tributaries enter. And, they may become even more unconfined during overbank flooding. Understandably, a mathematical model has yet to be devised that incorporates all these considerations. If we accept cross-sectional averages of velocity and water depth, then the other complexities can be represented with a relatively simple set of equations.

Like the flow of water in rivers, the flow of sediment in rivers is also unsteady and nonuniform at different scales of time and space. Sediment is temporarily stored in the stream bed and stream banks from flood to flood, or century to century, as sediment-feed rates and water discharges fluctuate. Even for a given water discharge rate, transport rates may vary considerably across a stream cross section as a function of secondary flows, local bed roughness, and upstream availability of different sediment particle sizes. This complexity has spawned hundreds of sediment transport equations.

Here we attempt to steer between an understandable but trivial fluvial model and a realistic but opaque one by following van Niekerk, Vogel, Slingerland, and Bridge (1992). First, we derive a two-dimensional fluid flow model from basic principles and present it with a simple application. Then, we discuss the physics of sediment entrainment and transport. Finally, we couple the fluid and sediment transport models through an equation describing conservation of the bed, demonstrating that the coupled model accurately predicts sediment transport rates and evolution of bed textures for various unsteady, nonuniform natural flows.

MODEL OF 2-D GRADUALLY VARIED FLOW IN A SINGLE THREAD CHANNEL

First, we derive the set of equations describing one-dimensional, steady, gradually varied flow. Although technically the equations describe steady flows (where depth, velocity, and discharge do not vary with time at a point), they also can be used without gross error to simulate the unsteadiness of flows over "geomorphic time." By geomorphic time is meant durations of hundreds to thousands of years such that a stream bed adjusts much more slowly than the flow in the stream. We assume that the effects of changes in cross-sectional area and bed slope on the flow within a timestep are negligible. The set of equations also is limited to *gradually varied* flows, which are nonuniform flows in which the boundary friction is dominant in determining the water surface's profile, in contrast to other forms of energy losses.

We begin with the set of equations describing the motion of an ideal fluid that was first published in 1755 by a key figure in eighteenth-century mathematics and the dominant theoretical physicist of that century: Leonhard Euler (*oiler*). Euler should be ranked with Archimedes, Newton, and Gauss, but for some curious reason is not well known outside mathematical circles. Euler was born near Basel, Switzerland, in 1707, and learned mathematics from John Bernoulli. He began to publish papers at eighteen, and through the next fifty-eight years poured forth a flood of contributions in calculus, differential equations, analytic and differential geometry of curves and surfaces, the theory of numbers, series, and the calculus of variations, all at the rate of about 800 pages per year. He created analytical mechanics. He investigated the bending of beams, the propagation of sound, and musical consonance and dissonance. His three volumes on optical instruments contributed to the design of telescopes and microscopes. He calculated the perturbative effect of celestial bodies on the orbit of a planet and the paths of projectiles in resisting media. And he was father of and teacher to thirteen children.

Euler's fundamental equations for the motion of an ideal fluid describe inviscid (i.e., nonviscous or frictionless) incompressible flow. They are simply an expression of Newton's general law of motion which says states that:

the total time rate of change of a system's momentum =
sum of forces acting on the system **(4-1)**

Defining *the system* in the case of fluids is facilitated by considering streamlines. Streamlines are continuous and smooth curves, everywhere tangent to the velocity vectors in a flow. By definition, they cannot cross, and at any given instant, there is only one set of streamlines for a particular flow. A bundle of streamlines collected together around a closed curve creates an elementary flow channel called a *stream tube*. A segment of a stream tube defines a convenient system to which the general law of motion can be applied.

To derive Euler's equations, consider the fluid in a segment of a stream tube (Figure 4-1). Because density times volume is mass, and mass times velocity is momentum, the time rate of change of the fluid's momentum in the s direction is:

$$\frac{d}{dt}(\rho dA ds V_s) = \frac{d}{dt}(\rho V_s)\, dA ds \qquad \textbf{(4-2)}$$

where: ρ = fluid density,
$dAds$ = differential volume of fluid in segment,
V_s = s-directed fluid velocity.

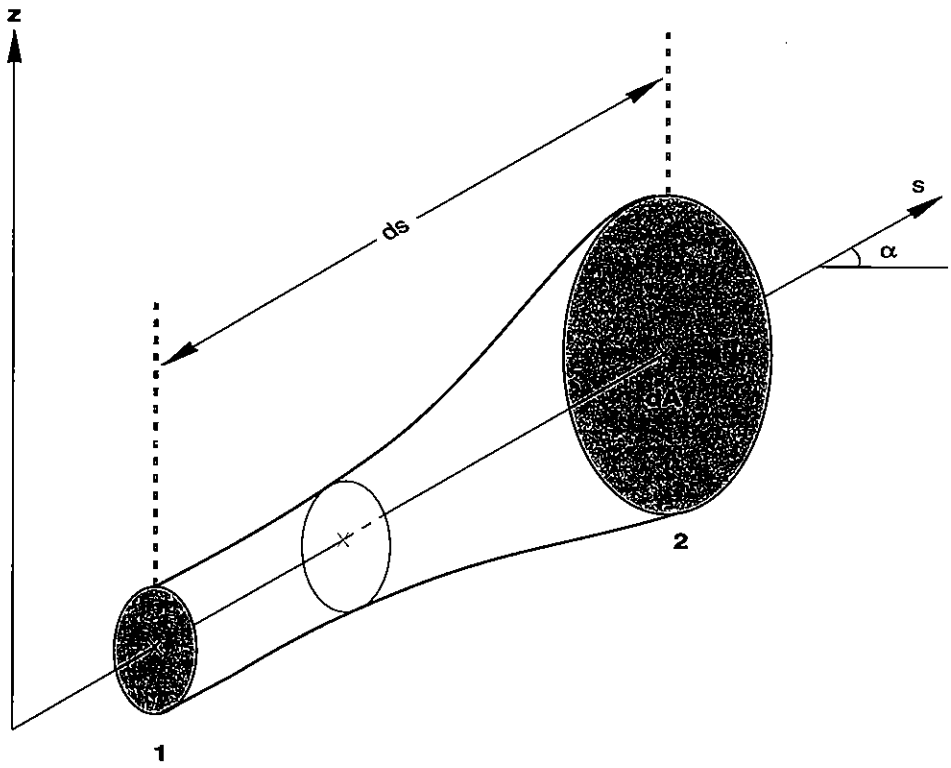

Figure 4-1 Derivation of Euler's equation by application of Newton's general law of motion to fluid in a stream tube. Angle between s axis and horizontal is α.

Euler considered the important forces acting on the fluid in the tube segment to be pressure forces and gravity forces. The net pressure force acting in the s direction is the difference between the pressures forces on faces 1 and 2 (Figure 4-1). Let us define the pressure at face 1 as p. The pressure at face 2 can be defined in terms of the pressure at face 1, thanks to Taylor's Theorem (3-3), as:

$$p + \frac{\partial p}{\partial s} ds \tag{4-3}$$

and the difference in pressure forces between the two faces, called the net pressure force, is:

$$\text{net pressure force} = -\frac{\partial p}{\partial s} dA ds \tag{4-4}$$

where dA converts a pressure to a pressure force.

The gravity force on the fluid in the tube, resolved in the s direction, is $\rho g dA ds \sin\alpha$. Defining $\sin\alpha$ in terms of s and z ($\sin\alpha = \frac{\partial z}{\partial s}$), this becomes:

$$s\text{-directed gravity force} = -\rho g \frac{\partial z}{\partial s} dA \tag{4-5}$$

Assembling (4-2), (4-4), and (4-5), according to the general law of motion (4-1), and assuming that fluid density does not vary in space or time, yields:

$$\frac{d}{dt}(\rho V_s)\,dAds = -\frac{\partial p}{\partial s}dAds - \rho g\frac{\partial z}{\partial s}dAds \tag{4-6}$$

which, for an incompressible fluid such as water, simplifies to:

$$\frac{dV_s}{dt} = -\frac{1}{\rho}\frac{\partial}{\partial s}(p+\rho gz) \tag{4-7}$$

Next, the total time derivative, $\frac{dV_s}{dt}$, can be expanded to reveal its two parts: an acceleration because of passage of time and an acceleration because of the fluid's movement through space. This may be better understood by conducting the following "thought experiment." Consider the changes in outside air temperature traveling by car from Pennsylvania to Florida in the winter, departing in early morning. The total change in temperature is a change with respect to time as the sun heats up the air during the day, plus the change with respect to distance as the car travels towards lower latitudes where the climate is warmer. The latter rate of change is a function of the speed of the car. Therefore, the total change may be written as:

$$\frac{dT}{dt} = \frac{\partial T}{\partial t} + V_c\frac{\partial T}{\partial s} \tag{4-8}$$

where V_c = speed of car.

Similarly, the total acceleration of a fluid particle in moving along a streamline in Figure 4-1 is:

$$\frac{dV_s}{dt} = \frac{\partial V_s}{\partial t} + V_s\frac{\partial V_s}{\partial s} \tag{4-9}$$

Substituting (4-9) into (4-7) yields the Euler equation of acceleration for an ideal incompressible fluid:

$$\frac{\partial V_s}{\partial t} + V_s\frac{\partial V_s}{\partial s} = -\frac{1}{\rho}\frac{\partial}{\partial s}(p+\rho gz) \tag{4-10}$$

The next step in deriving the gradually varied flow equation is to integrate Euler's equation, thereby gaining Bernoulli's equation (named after Daniel Bernoulli, the son of Euler's mathematics teacher, John Bernoulli). The integration is easy if the second term in (4-10) is written as $\frac{\partial}{\partial s}\left(\frac{V_s^2}{2}\right)$ using the chain rule. Then (4-10) becomes:

$$\rho\frac{\partial V_s}{\partial t} + \frac{\partial}{\partial s}\left(\frac{\rho V_s^2}{2} + p + \rho gz\right) = 0 \tag{4-11}$$

If the flow is steady, the local acceleration (first term) is zero, and integration over s yields Bernoulli's equation:

$$\frac{\rho V_s^2}{2} + p + \rho g z = f(t) \tag{4-12}$$

Because this is an integration of a partial differential, it yields a *function* of integration. It is a function of time, because although the velocity was assumed to remain constant with time at all points in the flow, we place no such restriction on temporal variation in the pressure intensity.

Bernoulli's equation is one of the most useful relationships in fluid dynamics. In its above form it states that the kinetic energy of a flow, embodied by the V^2 term, varies inversely along a streamline with the potential energy, as embodied by the pressure and gravity terms. As fluid velocity increases, pressure decreases, which is why planes fly, volleyballs with top-spin dive to the floor, and pebbles on a stream bed are lifted.

Dividing all terms by ρg, we see that Bernoulli's equation demands that the fluid pressure, elevation, and velocity heads along a streamline in an inviscid (frictionless) flow sum to a constant:

$$\frac{p}{\gamma} + z + \frac{V^2}{2g} = H_T \tag{4-13}$$

where: p = fluid pressure at point along streamline,
γ = fluid specific gravity,
z = elevation of point above datum,
V = fluid velocity (with subscript s dropped for generality),
g = gravitational acceleration,
H_T = total head.

The terms are called heads because they have units of distance. It is this form that describes open channel flow.

Now, consider a streamline in the x-direction along the bed (Figure 4-2). Assume that the pressure is hydrostatic in the channel, such that the pressure in the streamline is:

$$p = \gamma y \tag{4-14}$$

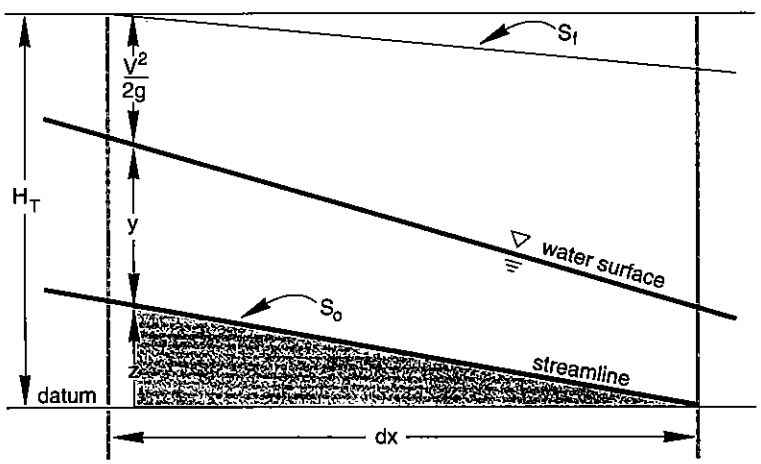

Figure 4-2
Longitudinal section through hypothetical open channel showing application of Bernoulli's equation to an open channel.

allowing us to write:

$$y + z + \frac{V^2}{2g} = H_T \tag{4-15}$$

This assumption means that bed slopes must be less than about 0.01, because at steeper slopes the bed is not orthogonal to the gravity acceleration vector. Also, the vertical fluid accelerations must be negligible.

Now (4-15) does not include frictional losses, because Bernoulli's equation was derived for an ideal (inviscid) fluid. The common (and quite correct) treatment to overcome this inadequacy is to define a rate of head loss with distance due to friction as:

$$\frac{dH_T}{dx} = -S_f \tag{4-16}$$

where: S_f = friction slope or slope of energy grade line.

Then, from (4-15) and (4-16):

$$\frac{d}{dx}(z + y + \frac{V^2}{2g}) = -S_f \tag{4-17}$$

or,

$$\frac{d}{dx}(y + \frac{V^2}{2g}) = S_o - S_f \tag{4-18}$$

where the bed slope S_o is defined as:

$$S_o = -\frac{dz}{dx} \tag{4-19}$$

How are frictional losses, represented by the friction slope S_f, estimated? First, it can be shown for both uniform and nonuniform flows that:

$$\tau_o = \rho g R S_f \tag{4-20}$$

where: τ_o = mean longitudinal shear stress acting over perimeter of channel,
R = hydraulic radius of channel,
S_f = slope of total energy line or friction slope.

This expression arises from a force balance on a parcel of fluid in the channel. If the fluid is not accelerating, then the resisting force per unit area, given by τ_o, must equal the downslope force per unit area due to gravity, which is the right-hand side of (4-20), if sin α is approximated by tan α, which is S_f. Now, as first pointed out by Newton:

$$\tau_o = a\rho V^2 \tag{4-21}$$

where: a = coefficient of drag (a dimensionless estimator of friction)
V = an appropriately chosen velocity (in this case the cross-sectional average).

Equating (4-20) and (4-21), and solving for S_f yields:

$$S_f = \frac{V^2}{C^2 R} \tag{4-22}$$

where: $C = \sqrt{\frac{g}{a}}$.

C is the Chezy constant with units of $m^{1/2}$/time, named after the French engineer who introduced it in 1768 while designing a canal for the Paris water supply. Observation of flows in rivers and canals by the 1870s led to the conclusion that C was proportional to the 1/6th power of the hydraulic radius (defined as cross-sectional area divided by wetted perimeter), with the proportionality "constant" being a function of bed roughness. In 1891 a Frenchman wrongly attributed this relationship to an Irishman, R. Manning, and expressed it in the form:

$$C = \frac{R^{\frac{1}{6}}}{n} \tag{4-23}$$

where n is now called Manning's n and is solely a characteristic of channel roughness. The units of n are $m^{1/6}$. Alternatively, one can express the Chezy C as $\sqrt{8\frac{g}{f}}$, where f is the dimensionless Darcy-Weisbach friction coefficient.

Finally, substituting (4-22) in (4-18), yields the gradually varied flow equation, an ordinary nonlinear differential equation:

$$\frac{d}{dx}\left(y + \frac{V^2}{2g}\right) = S_o - \frac{V^2}{C^2 R} \tag{4-24}$$

There are two unknowns in (4-24), flow velocity V, and water depth or stage y, and therefore another equation is necessary before (4-24) can be solved uniquely. As is commonly the case, the other equation arises from the principle of mass conservation:

$$Q = VA(y) \tag{4-25}$$

where: Q = water discharge,
A = cross-sectional area of channel (and therefore dependent upon y).

In principle, (4-24) and (4-25) may be solved for V and y as functions of x, given Q, C, S_o, and the channel's hydraulic geometry as it may vary in x. In practice, there is no known analytical solution for irregular cross sections, and the equation set is solved using one of several finite difference formulations. The scheme presented here is the step method of Henderson (1966).

Consider a typical application as depicted in Figure 4-3. A stream channel has been surveyed to yield a number of cross sections, thus allowing calculation of cross-sectional areas and hydraulic radii as functions of water stage or depth. In addition, the plan of the channel is known, thus allowing bed slopes to be calculated. Chezy C is also known for each section, having been obtained by estimating Manning's n from tabulated values (e.g. Henderson, 1966, Table 4-2). For any particular water discharge and known flow depth at one cross section, the problem is to calculate flow depths and velocities at other cross sections. This may be accomplished by stepping along the channel, one cross section at a time, using known values of V and y at adjacent cross section JN to calculate the unknown

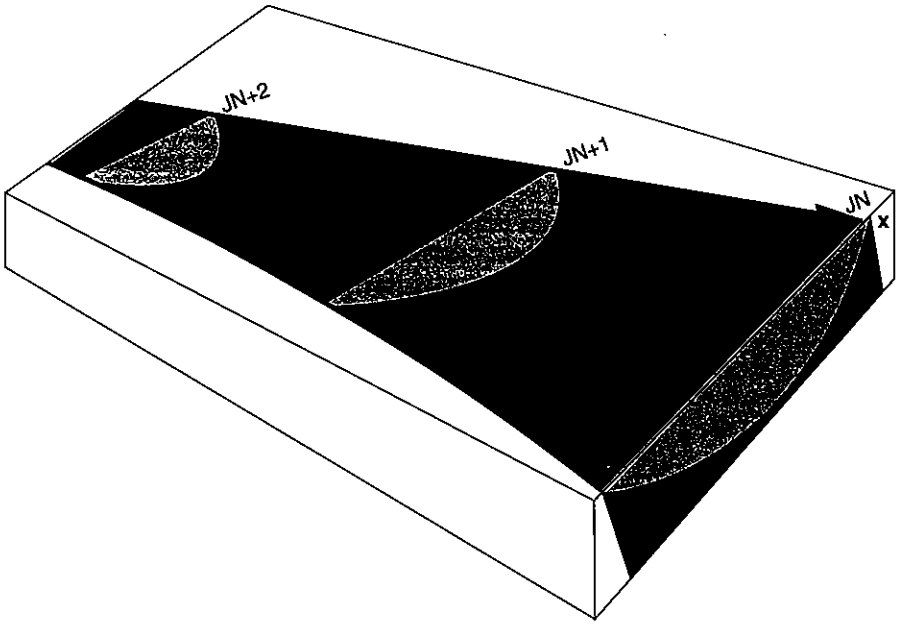

Figure 4-3 Example application of the gradually varied flow model. JN is the section number at the present stage in the computation.

values at cross section JN+1. Let JN=1 and assume that the dependent variables are known there. At section JN+1 and subsequent cross sections, (4-15) may be written as:

$$H_2 = y_2 + z_2 + \frac{V_2^2}{2g} \tag{4-26}$$

where z_2, the elevation of the bed, is known. If (4-16) is written in finite-difference form:

$$\frac{H_2 - H_1}{\Delta x} = -S_f \tag{4-27}$$

where: Δx = finite-distance between two sections,

it may be solved for H_2, yielding:

$$H_2 = H_1 - \Delta x S_f \tag{4-28}$$

Inasmuch as loss due to friction occurs between two cross sections, it is reasonable to calculate the loss as an average of the friction slopes at the two sections:

$$H_2 = H_1 - \frac{\Delta x}{2}(S_{f_1} + S_{f_2}) \tag{4-29}$$

Equations (4-26) and (4-29) give two expressions for H_2, and the aim of the computation is to equalize the two values. By guessing at a value of y_2, V_2 may be

calculated from (4-25) and S_{f_2} may be calculated from (4-22). Then, (4-26) and (4-29) may be evaluated and compared. If they are not equal, y_2 is adjusted and iteration proceeds until convergence. The trick in a numerical scheme is to adjust y_2 by an appropriate amount. By evaluating the conditions under which the error in H varies as a function of Δy_2, Henderson (1966) computed the adjustment as:

$$\Delta y_2 = \frac{H_e}{1 - \frac{V^2}{2gy} + 3S_f \frac{\Delta x}{2R_2}} \tag{4-30}$$

where H_e is the error, or difference between the H_2 calculated in (4-26) and (4-29).

The bootstrapping operation described above depends strongly upon the hydraulics of the initial stream cross section, and therefore its selection is not arbitrary. This may be seen by considering a special equation called the specific energy equation. If the datum is the stream bed, making z everywhere zero, and a discharge per unit width q is introduced such that $V=q/y$, then (4-15) becomes:

$$y + \frac{q^2}{2gy} = E \tag{4-31}$$

The constant E stands for specific energy.

Notice that for any particular specific energy and q, this equation is a quadratic in y and therefore possesses two solutions. These are the water depths of sub- and supercritical flow, separated by critical flow where $\frac{V^2}{\sqrt{gy}} = 1$. The latter expression is a dimensionless ratio called the Froude number, being the ratio of the speed of the flow to the celerity or speed of a shallow water wave (see Chapter 5 for more on wave speeds). In supercritical flows where the Froude number is greater than 1, a shallow water wave, or any hydraulic disturbance in general, cannot propagate upstream, because the medium is moving faster than the wave speed. The consequence of this is that *a supercritical flow can only be controlled from upstream, whereas a subcritical flow is best controlled from downstream.* Thus the initial cross section from which we launch the computations should be one which determines a particular depth-discharge relationship in the specific energy equation. The calculations described above should proceed upstream from this control section for subcritical flows, and must proceed downstream for supercritical flows. Typical engineering control sections are weirs and sluice gates. For our purposes they are artificial cross sections at the boundaries of the stream's reach. If by precalculation the flow is expected to be subcritical, the control section would be at the downstream end; if the flow is everywhere supercritical, then the control section would be placed at the upstream end of the model reach.

Equations (4-22) through (4-30) have been encoded in the FORTRAN program FLDTA (Program 4) for a variable width, rectangular channel. If an application involves irregularly shaped cross sections, functions or look-up tables must also be supplied that specify how cross-sectional area and wetted perimeter vary with stage at each cross section.

Table 4-1 Example input file for Experiment 4-1

10 1 100. 0.02	number of nodes; number of timesteps; Δx; n
10. 11. 12. 13. 14. 15. 16. 17. 18. 19.	cross section widths (m)
10. 9.9 9.8 9.7 9.6 9.5 9.4 9.3 9.2 9.1	elevations above datum (m)
900.0 1.0	location of control section and water depth (m)
25.0	discharge (m^3 s^{-1})

Experiment 4-1: An Example

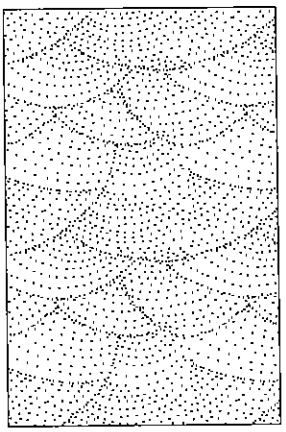

A reach of a straight, single-thread stream drops from 10 to 9.1 meters in elevation over a distance of 1000 meters while increasing linearly in width from 10 to 19 meters. The stream's discharge is uniformly 25 m^3 s^{-1}, and its bed consists of smooth mud with no weeds, providing a uniform Manning's n of about 0.02. Under these conditions, an initial calculation assuming uniform flow suggests the flow will be subcritical, and therefore the control section should be placed at the downstream end of the reach. For discussion, let us place it 900 meters down the reach. The reach is arbitrarily divided into eleven cross sections 100 meters apart, with widths and bed elevations given in Table 4-1.

The results are presented in Figure 4-4. The flow depths decrease slightly downstream and then increase to the prescribed value of 1 meter at the control section. The decrease arises due to the increasing stream width, and the increase arises because the control water depth demands it. Flow velocities decrease monotonically downstream due to the expanding stream width, but note that the decrease is nonlinear due to the interaction between the expanding cross section and backwater from the control water depth.

As mentioned earlier, although this algorithm is for steady flows, it can be applied to certain unsteady flows where the time step between calculations is large relative to the time interval of adjustment. For example, if the problem involves growth of an alluvial fan over thousands of years and the timestep is in decades, it is reasonable to calculate the flow using this model, erode and deposit sediment, adjust the bed elevation accordingly, and recalculate the flow using the new elevations. An example is given later in this chapter.

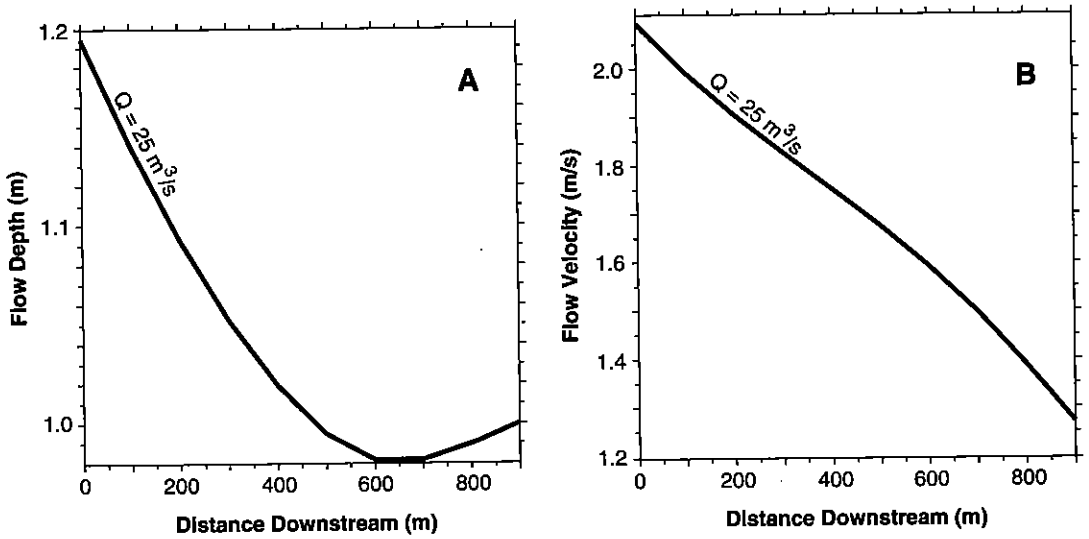

Figure 4-4 Plots of flow depth and velocity versus distance downstream obtained in Experiment 4-1. In (A) flow depth decreases downstream to the control section and then increases, whereas in (B) flow velocity decreases monotonically.

It could be argued that understanding the characteristics and origin of clastic strata requires understanding the physics of sediment transport. Given its importance, we present two formulations here for sediment transport. One is accurate, general, and complicated, whereas the other is less accurate but simple. The first can be used with little modification to predict the sediment load carried by turbulent, unidirectional flows, whether in rivers or epeiric seas. The other is restricted to open-channel unidirectional flows. We start with the first because it illustrates the physical principles that underlie sediment transport.

Transport of sediment grains can be broken down into four steps, each with its own mathematical characterization. First, sediment grains must be set into motion or entrained by a flow. The relationship between a grain's size, density, and pivot angle, and the strength of flow at which the grain begins motion is called the *entrainment criterion.*

Second, once in motion, grains travel either as bedload or suspended load, depending on the mechanism of grain support. Bedload refers to sliding, rolling, and saltating grains that are supported at least in part by collisions with other grains or by contact with the bed. In water these grains travel within a few grain diameters of the bed as a low-concentration dispersed grain flow. Suspended load, on the other hand, refers to grains supported by the mean upward-directed fluid impulses arising from eddy currents of turbulent flow. As might be expected, the two loads are calculated differently, and therefore it is necessary to know under what conditions a grain participates in each. In other words, we need a *suspension criterion.*

Third, after the grains are assigned either to bedload or suspended load, their *mass fluxes* must be calculated as a function of their availability in the bed, the bed geometry, and various properties of the flow such as the magnitude of the bed shear stress, the vertical velocity profile, and the water depth. As we shall see, this calculation requires mathematical specification of the distribution of *instantaneous bed shear stresses* and of the *vertical momentum transfer*, both of which arise from fluid turbulence.

Fourth and finally, spatial and temporal variations in entrainment and deposition cause a bed's texture, geometry, and composition to evolve. Because these changes influence the sediment transport, the *bed evolution* must be calculated from a bed continuity equation. The four steps and their mathematical characterizations are considered next in order.

Entrainment Criterion

As discussed above, predictions about sediment transport depend strongly upon the critical shear stress necessary to initiate motion of a specific size-density particle on a heterogeneous bed. Most sedimentology textbooks today present either the Shields or Hjulstrom relationship. Unfortunately, neither is appropriate for grains much larger or smaller than the median size of the bed, because neither relationship accounts for relative protrusion and grain-hiding effects. Recent work on entrainment has focused on rectifying this shortcoming.

Consider the torque balance on a grain of diameter D_i resting on grains of diameter D_{50}, which is the median size of the bed (Figure 4-5). The grain will begin to move, pivoting about point A, when the torque due to the fluid force F

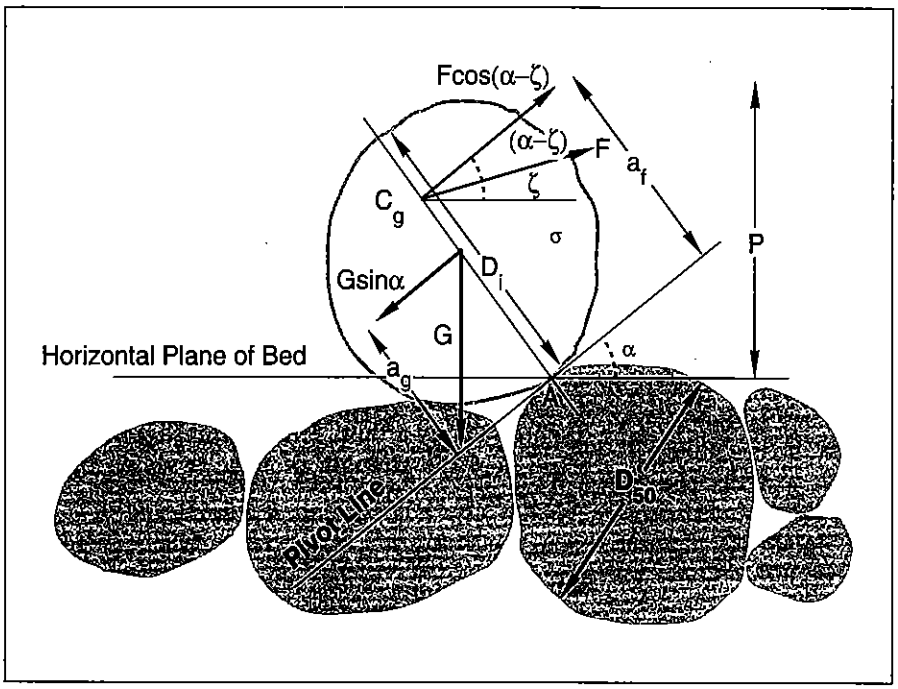

Figure 4-5 Torque balance on grain at threshold of motion. Symbols are defined as follows: F = fluid drag and lift forces, α = pivot angle, ζ = angle of fluid force vector with horizontal, C_g = center of gravity, G = grain submerged weight, D_i = diameter of *i*-th grain size, σ = grain density, a_f and a_g = moment arms, A = pivot point, P = protrusion height, and D_{50} = median grain size of bed.

just exceeds the torque due to the resisting force G. The torque around point A by fluid forces T_1 is given by:

$$|T_1| = Fa_f\cos(\alpha - \zeta) \tag{4-32}$$

where the variables are defined in Figure 4-5. The torque around point A due to the grain's weight T_2, is given by:

$$|T_2| = Ga_g\sin\alpha \tag{4-33}$$

The grain will begin to pivot when $|T_1| > |T_2|$, or:

$$\frac{F}{G} \geq \frac{a_g\sin\alpha}{a_f\cos(\alpha - \zeta)} \tag{4-34}$$

Now, the fluid force vector F is a vector sum of drag and lift forces on the grain. These can be approximated by the quadratic equation:

$$F = (C_D + C_L)\,\rho A \frac{V^2}{2}\bigg|_{y = aD_i} \tag{4-35}$$

where: $(C_D + C_L)$ = coefficients of drag and lift respectively,

ρ = fluid density,

A = cross-sectional area of the grain exposed to the flow, here taken to be bD_i^2,

V = flow velocity at height $y=aD_i$, off bed,

a = unknown fractional constant.

The resisting force G is given by:

$$G = cD_i^3\,(\sigma - \rho)\,g \tag{4-36}$$

where: c = a constant,

σ = grain density.

Substituting (4-35) and (4-36) in (4-34) and rearranging yields:

$$V_c|_{z = aD_i} = \left[\frac{\sin\alpha}{\cos(\alpha - \zeta)}\,\frac{a_g}{a_f}\,\frac{(\sigma - \rho)}{\rho}\,\frac{2c}{b}\,\frac{1}{(C_D + C_L)}\right]^{\frac{1}{2}} \sqrt{gD_i} \tag{4-37}$$

where: V_c = critical flow velocity at height $z = aD_i$ above bed necessary for entraining grain of diameter D_i.

Next, this flow velocity near the bed must be related to a more practical measure of flow strength, such as the vertical mean flow velocity, or more desirably, the spatial and temporal average bed-shear stress, τ_o. This is accomplished by using the Prandtl equation, which describes the velocity structure of a turbulent flow in the proximity of a wall. Prandtl, a legendary German fluid dynamicist of the 1920s, concluded that the temporal mean velocity in the lower 20 percent of a flow above the thin viscous sublayer is given by:

$$V = A\sqrt{\frac{\tau_o}{\rho}}\,\ln\left(\frac{z}{k}\right) \tag{4-38}$$

where: $\sqrt{\frac{\tau_o}{\rho}}$ = shear velocity = U_* for convenience,

A = 2.5 for clear water,

z = distance measured away from wall,

k = roughness length for wall.

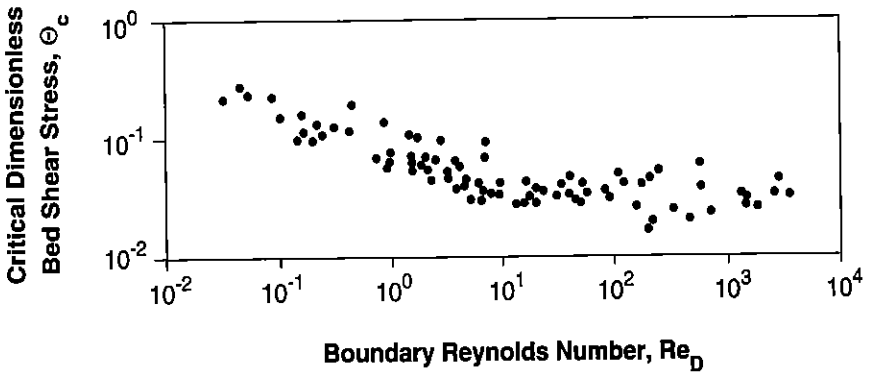

Figure 4-6 Shields diagram as presented by Miller et al. (1977), in which critical dimensionless bed shear stress, Θ_c, is plotted versus boundary Reynolds number, Re_D.

Substituting (4-38) into (4-37) for V_c and rearranging yields:

$$\frac{\tau_{o_c}}{(\sigma-\rho)gD_i} = \left\{a_g \frac{1}{C_D+C_L} \frac{1}{\left[Aln\left(\frac{aD_i}{k}\right)\right]^2} \frac{2c}{b} a_f^{-1}\right\} \frac{\sin\alpha}{\cos(\alpha-\zeta)} \qquad (4\text{-}39)$$

The left side has of (4-39) has been grouped in this form because it is a dimensionless ratio of the tangential force-per-unit-area exerted on the bed by the turbulent flow to the weight-per-unit-area of a grain layer 1 grain-diameter thick. It makes sense that above some threshold of bed-shear stress scaled to the weight of the grains, motion will commence. This ratio is often called the Shields parameter after A. Shields, the German hydraulic engineer whose work is important here. Shields parameter is usually given the label Θ_c. In a simple world, one might expect Shields parameter to be constant, but it is not. The terms within the braces on the right-hand side are complex functions of the structure of flow turbulence near the wall. The remaining terms involve α and the ratio of D_i to the length of the roughness elements. Let us first look at the dependence of critical shear stress on the structure of flow turbulence, by assuming that the bed consists of grains of only one size.

Bed of Homogeneous Size

In 1936, Shields published a landmark paper entitled *Anwendung der Ahnlichkeitsmechanik und der Turbulenzforschung auf die Geschiebebewegung*, which roughly translated means *Application of the Similarity Principle and Turbulence Research to Particle Movement*. In it, Shields established for the first time the functional form of (4-39) for the simplified case of homogeneous sizes. His results, along with more recent data, are plotted in Figure 4-6. To represent the

structure of the turbulent flow, he chose a dimensionless parameter called the boundary Reynolds number Re_D, defined as:

$$Re_D = \frac{U_* D}{\nu} \tag{4-40}$$

where: ν = fluid kinematic viscosity,

D = grain diameter of the unisize bed.

Note that Θ_c decreases and then slightly increases with increasing Re_D, becoming constant at 0.045 for $Re_D > 60$, that is, when the bed is hydraulically rough. Unfortunately, τ_o occurs in both Θ_c and Re_D, making it difficult to determine the dimensional critical shear stress of a particular size-density grain. This problem is overcome by approximating the curve in Figure 4-6 by three regression equations in the manner of Bridge (1981):

$$\Theta_c = (0.1Re_D)^{-0.3} \qquad \text{for } Re_D < 1 \tag{4-41}$$

$$\ln\Theta_c = -2.26 - 0.905\ln(Re_D) + 0.168\ln^2(Re_D) \qquad \text{for } 1 < Re_D < 60 \tag{4-42}$$

$$\Theta_c = 0.045 \qquad \text{for } Re_D > 60 \tag{4-43}$$

The above entrainment equations for a homogeneous bed have been encoded in the FORTRAN subroutines listed in Program 5.

Heterogeneous Size-Density Bed

How do we treat the case where the bed consists of a range of grain sizes? From Figure 4-5 we see that the terms in (4-39) dealing with relative grain sizes must be functions of D_i and grains of diameter D_{50}, because if the bed-size distribution is unimodal, D_i most probably will be resting on D_{50}, the median size of the distribution and the size that determines the bed roughness. We expect that if D_i is small with respect to D_{50}, then from (4-39), the critical Shields parameter Θ_c for the D_i size fraction of a mixture will be greater than Θ_c for the case of a homogeneously sized bed.

To account for this dependence, we adopt an empirical formulation for relative size terms provided by Komar (1987a; 1987b). Komar represents the relative grain size terms in (4-39) by a power function of the ratio D_i/D_{50} such that:

$$\Theta_{c_{ij}} = \Theta_{c_{50}}\left(\frac{D_{ij}}{D_{50}}\right)^{-m} \tag{4-44}$$

where: $\Theta_{c_{50}}$ = critical Shields parameter for median size,

D_{ij} = grain size of ith size fraction of the jth density species,

D_{50} = median bed grain size,

m = a constant.

Notice that the terms within the braces in (4-39) are represented by the critical Shields parameter for the median size, and the other terms are represented by the power function. As mentioned earlier, the Shields parameter is a dimensionless ratio of the bed shear stress to the immersed weight of a single layer of grains over a unit area. Here we define $\Theta_{c_{ij}}$ as:

$$\Theta_{c_{ij}} = \frac{\tau_{c_{ij}}}{(\sigma_j - \rho)\, g D_{ij}} \tag{4-45}$$

in which $\tau_{c_{ij}}$ is the critical bed shear stress necessary to entrain a grain of the ith size fraction of the jth mineral species. The magnitude of $\Theta_{c_{50}}$ is obtained from (4-41) to (4-43).

A matter of recent dispute has been the appropriate value of m in (4-44) (Parker, Klingeman, and McLean, 1982). For gravel of a unimodal distribution in which the range of sizes falls between $0.3 < D_{ij}/D_{50} < 22$, a good choice for m is 0.6 (Figure 4-7). For sand sizes, van Niekerk et al. (1992) found that if m is 0.65, acceptable results are obtained. Equation (4-44) and supporting relationships have been encoded in the FORTRAN subroutine ENTRAINH in Program 6.

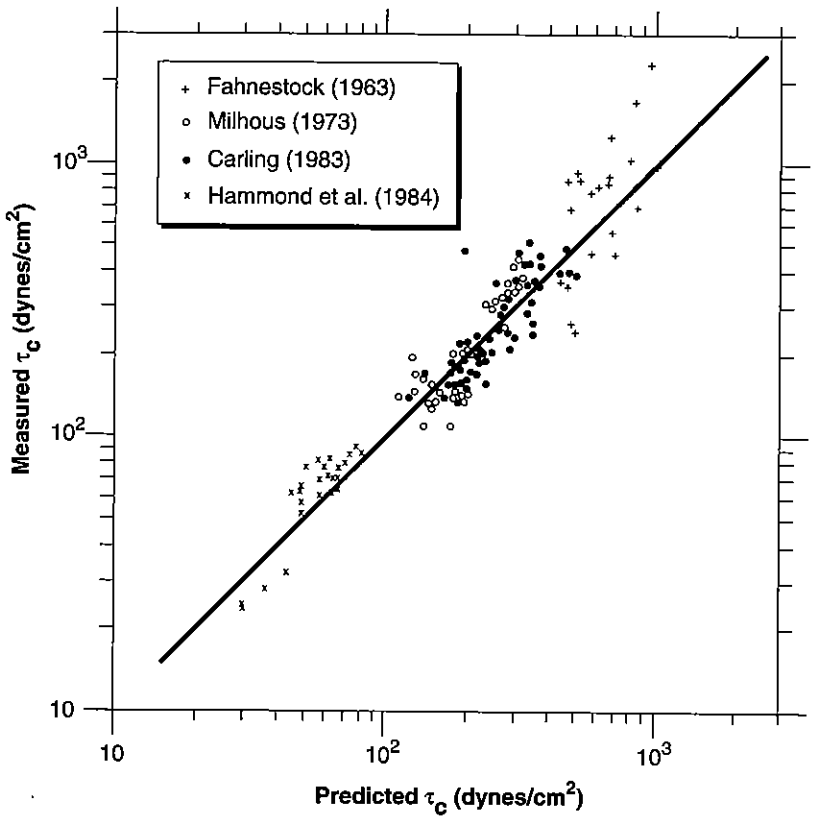

Figure 4-7 Log-log plot comparing measured and predicted critical bed shear stresses, τ_c, for entrainment of gravel from bed of mixed particle sizes (from Komar, 1987b).

Suspension Criterion

Having calculated which grains will be in motion, we must determine whether they will travel as bedload or suspended load. The criterion in general use assumes that grains will be suspended when the temporal mean turbulent lift force on the bedload per unit bed area F_{TL} slightly exceeds the grains' immersed weight per unit bed area, W', or:

$$\frac{F_{TL}}{W'} \geq 1 \tag{4-46}$$

By the general drag force equation:

$$F_{TL} = C_L A_L \rho \frac{(v'_u - v'_d)^2}{2} \tag{4-47}$$

where: C_L = a lift coefficient,
A_L = the area of grains exposed to lift per unit bed area,
ρ = fluid density,
v' = root mean squares of upward and downward turbulent fluctuations.

Experimental and theoretical studies (discussed in Bridge and Bennett, 1992) have concluded that this difference in magnitude of turbulent fluctuations near the bed is proportional to the temporal mean bed shear stress, τ_o, or more precisely, to its surrogate, shear velocity, U_*:

$$v'_u - v'_d = B\sqrt{\frac{\tau_o}{\rho}} = BU_* \tag{4-48}$$

where: B = proportionality constant.

Therefore,

$$F_{TL} = C_L A_L \rho \frac{B^2 U_*^2}{2} \tag{4-49}$$

Now consider a definition of the grains' immersed weight, W'. We could define the immersed weight of grains in terms of their density and volume, and enter it directly into (4-46), but there is a more elegant method. When grains settle at their constant terminal fall velocity w, the fluid drag acting on them must just equal their immersed weight:

$$C_{DS} A_L \rho \frac{w^2}{2} = W' \tag{4-50}$$

where: C_{DS} = coefficient of drag of grain settling in still water,
A_L = cross-sectional area of grain,
W' = grain's submerged weight.

It is the left-hand side of (4-50) which we substitute into (4-46), along with (4-49). Assuming that C_L equals C_{DS} yields:

$$w \leq BU_* \tag{4-51}$$

This elegant inequality states that the fall velocity of a gain must be less than a fixed proportion of the fluid shear velocity for a grain to be suspended. We will find it more convenient to express the criterion as the condition for a grain to *remain in the bedload.* With the possibility of i different sizes and j different densities, the suspension criterion then becomes:

$$\tau_{s_{ij}} < \frac{\rho w^2_{ij}}{B^2} \tag{4-52}$$

where: $\tau_{s_{ij}}$ = minimum shear stress necessary to cause suspension of ith size and jth density fraction of bed.

Theory and experiment show that B ranges from 1.25 to 0.64 and is set at 0.8 here.

Calculation of Fall Velocities

It is clear above that we must also know the constant terminal settling or fall velocities of sedimentary grains in a turbulent fluid. Accepting the common assumption that fall velocities in wall-bounded turbulent flows equal those in still water allows us to use an empirical equation due to Dietrich (1982). Based on the data (gray band) in Figure 4-8, he combined the fall velocities of grains with many different sizes, densities, and shapes into one nonlinear regression equation:

$$\begin{aligned}\log W_* = &-3.76715 + 1.92944\,(\log D_*) \\ &- 0.09815\,(\log D_*)^2 - 0.00575\,(\log D_*)^3 + 0.00056\,(\log D_*)^4\end{aligned} \tag{4-53}$$

$$W_* = \frac{\rho w^3_{ij}}{(\sigma_j - \rho)\, g \nu} \tag{4-54}$$

$$D_* = \frac{(\sigma_j - \rho)\, g D^3_{nij}}{\rho \nu^2} \tag{4-55}$$

where: W_* = dimensionless settling velocity,
D_* = dimensionless grain diameter,
ρ = fluid density,
w_{ij} = fall velocity of ith size and jth density particle,
σ_j = mineral density of jth fraction,
g = gravitational acceleration,
ν = kinematic viscosity,
D_{nij} = nominal diameter of ith grain size fraction and jth mineral density fraction obtained from sieve measurements.

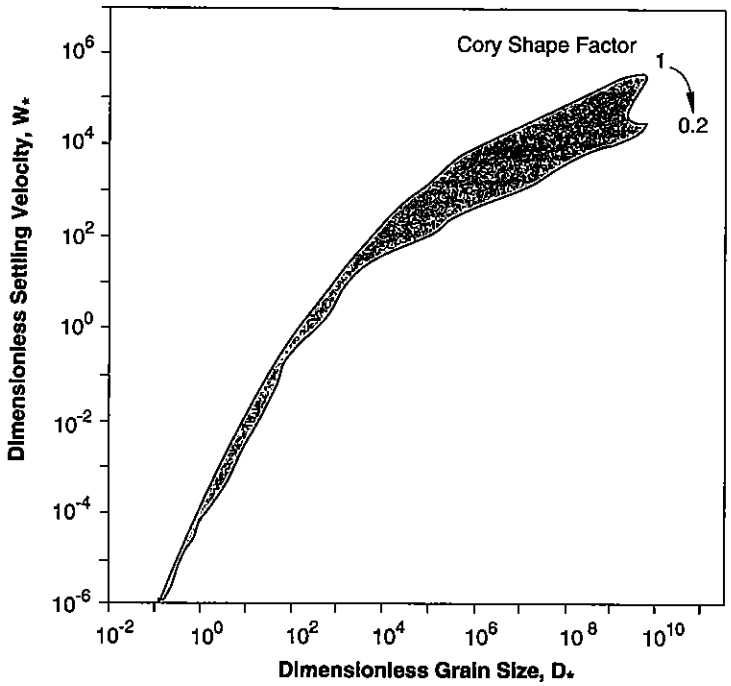

Figure 4-8 Log-log plot of dimensionless constant terminal settling velocity in still water versus dimensionless grain size as compiled by Dietrich (1982). Dimensionless settling velocity W_* is defined as $\rho \frac{w_{ij}^3}{(\sigma - \rho) g \nu}$, and dimensionless grain size D_*, is defined as $\frac{(\sigma - \rho) g D_{nij}^3}{\rho \nu^2}$, where *ij* and *nij* are subscripts as in the definitions for (4-55). Gray area marks cloud of data points. Grains with lower Cory shape factors plot lower in the cloud.

Program 7 contains a FORTRAN subroutine which calculates fall velocities from the Dietrich equation.

Sediment Load Formulation

There are scores of formulas that attempt to predict the flux of sediment by a unidirectional open channel flow, and none is entirely satisfactory. To understand why, the reader should refer to discussions in compendia such as those of Mutlu Sumer and Muller (1983) and Raudkivi (1990). For our purposes, a formula will be sufficient if it is theoretically based, conceptually simple, and accurate over a useful range of grain sizes and flow strengths. In addition, it must predict the transport rate of each grain size separately. The Bagnold equation, as modified by Bridge and Dominic (1984), is a good place to start.

Bedload Formula

The modified Bagnold bedload transport formula (Bridge and Dominic, 1984) is:

$$i_{b_{ijk}} = W_{ij}\frac{B}{\tan\alpha}(U_*-U_{*_{c_{ij}}})(\tau_o-\tau_{c_{ij}}) \qquad \textbf{(4-56)}$$

where: $i_{b_{ijk}}$ = bedload transport rate (weight transported per unit width per unit time) of ith size and jth density fraction during application of kth instantaneous bed shear stress,

W_{ij} = volumetric proportion of ith-jth fraction in active bed,

$B = \frac{1}{\kappa} ln(\frac{z}{k_f})$,

κ = von Karman's constant,

z = distance above bed to center of fluid thrust on bedload grains,

kf = bed roughness,

$\tan\alpha$ = dynamic friction coefficient,

U_* = effective instantaneous fluid shear velocity,

τ_o = effective instantaneous bed shear stress.

The subscript c stands for critical value at moment of entrainment. Experiments show that $B/\tan\alpha$ is roughly a dimensionless constant equal to 10, and this value will be used here.

Now, notice that it is the *effective* fluid shear velocity and shear stress that are called for. By "effective" we mean that portion of the fluid shear stress exerted on the bed and banks that is *available to transport sediment.* Fluid shear stress arising from flow separation over dunes is not effective in transporting sediment, and therefore should not be included in (4-56). Hans Albert Einstein ("the son") proposed a method for defining effective shear stress by thinking of the total hydraulic radius at a site as the sum of two components, one creating skin friction, R'', which is the effective part, and the other creating form friction, R' (Einstein, 1950). The former can be substituted in (4-20) to define an effective shear stress, $\bar{\tau}_o''$. By definition the effective temporal mean shear velocity, U_*'', is:

$$U_*'' = \sqrt{\frac{\bar{\tau}_o''}{\rho}} = \sqrt{gR''S_f} \qquad \textbf{(4-57)}$$

Einstein used the empirical observation that the average fluid velocity at a stream cross section, $\bar{V}$, is given by:

$$\frac{\bar{V}}{U_*''} = 5.75\log\left(\frac{12.27}{\frac{k}{R''}}\right) \qquad \textbf{(4-58)}$$

where: U_*'' = effective temporal mean shear velocity,

k = grain roughness, assumed to be 2.5 times representative size of bed particles.

Thus, given the average velocity and friction slope from a flow model as that in Program 4, and given a bed-grain size, (4-57) and (4-58) can be solved iteratively

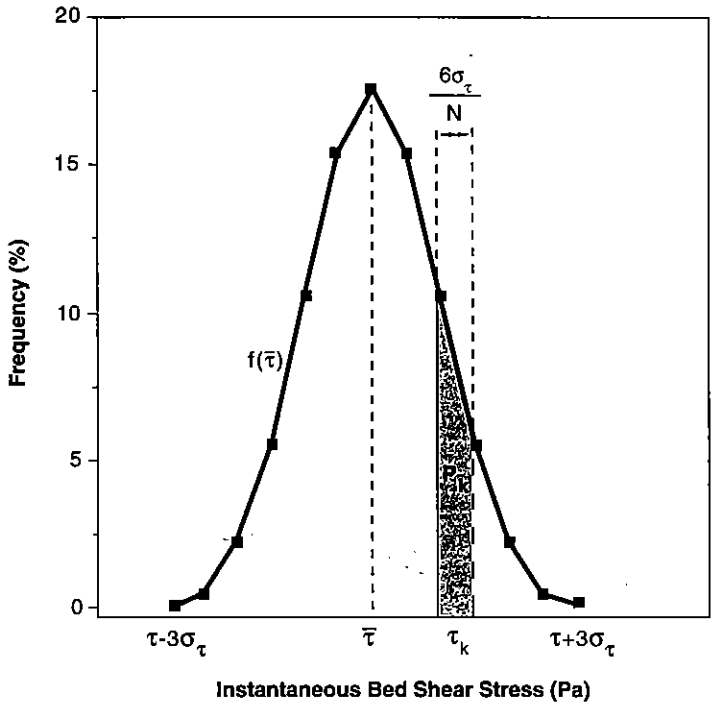

Figure 4-9
Example frequency distribution of instantaneous bed shear stress with mean $\bar{\tau}$, and standard deviation σ. Small rectangle denotes calculated frequency class.

for R'' and thus U_*'' and τ_o''. Henceforth, references to shear stress and velocity assume that these skin-friction components apply unless otherwise noted, and the $''$ superscript will be dropped. A FORTRAN subroutine which calculates effective shear velocities is give Program 8.

Next, note that it is the *instantaneous* shear velocities and stresses that are used in (4-56). It has long been established that flow turbulence results in fluctuation of local instantaneous bed shear stresses about a mean value due to the continuous disruption of the local boundary layer by turbulent bursts and sweeps. Because the modes and rates of sediment transport vary as a function of these turbulent events, it is desirable to incorporate a distribution of instantaneous bed shear stresses in our bedload transport model. Observations suggest that instantaneous bed shear stresses approximate a Gaussian distribution (Figure 4-9) for fully turbulent flow, with a coefficient of variation of 0.4:

$$f(\tau_o) = \frac{1}{\sigma_{\tau_o}\sqrt{2\pi}} e^{-\frac{1}{2}\left[\frac{(\tau_o - \bar{\tau}_o)}{\sigma_{\tau_o}}\right]^2} \qquad \textbf{(4-59)}$$

where: τ_o = instantaneous mean bed shear stress,

$\bar{\tau}_o$ = temporal mean bed shear stress,

σ_{τ_o} = standard deviation of instantaneous bed shear stress distribution.

To incorporate turbulent fluctuations into the bedload model, let us calculate the bedload transport rate of each size-density fraction for each of N bed-shear stress ranges. Each range will have a mean value of τ_{ok}, and a width $\Delta\tau_o$ equal to $6\sigma_{\tau_o}/N$ (Figure 4-9). The proportion of time allotted to each shear stress range P_k

is obtained by integrating the distribution function over the interval $\Delta\tau_o$. Program 9 lists a FORTRAN subroutine that calculates frequency distributions of instantaneous bed-shear stresses.

Incorporating all of these ideas leads to the final form of the bedload transport equation:

$$i_{b_{ijk}} = KW_{ij}P_k(U_* - U_{*_{c_{ij}}})(\tau_o - \tau_{c_{ij}}) \quad \textbf{(4-60)}$$

where: $i_{b_{ijk}}$ = bedload transport rate (weight transported per unit width per unit time) of ith size and jth density grain due to kth instantaneous shear stress interval,
K = 10,
W_{ij} = volumetric proportion of ith-jth fraction in active layer,
P_k = proportion of time kth shear stress is active,
c = subscript for critical values at moment of entrainment.

To obtain the total transport rate of the ith-jth fraction, (4-60) is summed over all instantaneous bed shear stresses for which the fraction is in motion as bedload:

$$i_{b_{ij}} = \sum_{k=e}^{f} i_{b_{ijk}} \quad \textbf{(4-61)}$$

where: e = interval of smallest instantaneous shear stress greater than $\tau_{c_{ij}}$,
f = interval of largest instantaneous shear stress less than or equal to $\tau_{s_{ij}}$.

Program 10 lists a FORTRAN subroutine incorporating these ideas. It calls a subroutine named DRANGEH to calculate e and f, the bounds of summation in (4-61).

Suspended Load Transport

Having calculated the bedload, we can now calculate the suspended load. The suspended load is the width- and depth-integrated distribution of suspended solids carried forward by a turbulent flow. It is defined as:

$$S_{s_{ij}} = b\int_{a}^{D} V_x C_{ij}\,dz \quad \textbf{(4-62)}$$

where: S_s = suspended load transport rate (kg s^{-1}),
b = width of flow (m),
V_x = x-directed fluid velocity at height z (m s^{-1}),
C = concentration of suspended solids at height z (kg m^{-3}),
D = depth of flow (m), as defined in Figure 4-10.

As in other formulations, we assume that the boundary between the bedload and suspended load occurs at the top of a moving bed layer, at distance $z = a$ from the reference plane. We then define a velocity profile, $V_x(z)$, and a concentration profile, $C_{ij}(z)$, over the vertical. The vertical velocity profile of turbulent, uniform,

wall-bounded flows is well described by the von Karman-Prandtl mixing-length model of turbulence. This model produces a logarithmic profile, which written in terms of the mean flow velocity over the vertical, is:

$$V_x(z) = \frac{U_*}{\kappa}\left[ln\left(\frac{z}{D}\right) + 1\right] + \bar{V} \qquad \textbf{(4-63)}$$

where: U_* = effective temporal mean shear velocity,
κ = von Karman constant (0.4 for clear water),
z = height above bed,
D = water depth,
$\bar{V}$ = temporal and vertical mean velocity.

The FORTRAN subroutine in Program 11 computes values of V_x as functions of the independent variables.

Suspended sediment concentrations for individual size-density fractions usually are calculated from the convection diffusion equation for the vertical distribution of suspended sediment. The convection diffusion equation is derived from

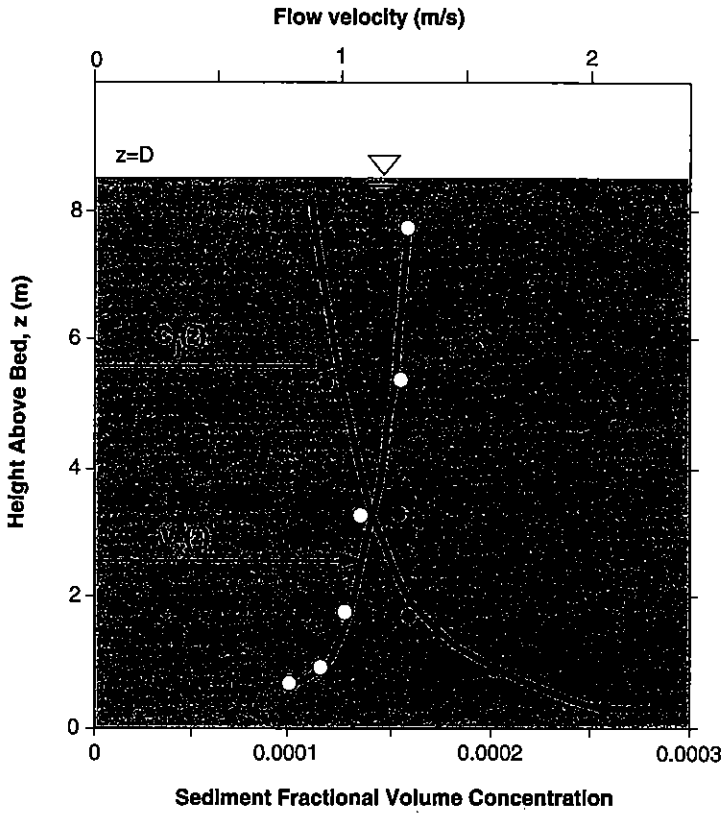

Figure 4-10 Plots of (A) height above stream bed versus concentration of suspended sediment (solid circles) and (B) height versus flow velocity (open circles) in Mississippi River at St. Louis observed by Colby (1963).

a mass balance for suspended sediment by assuming that steady state conditions apply over a time step, that the dependent variables are constant in the cross-stream, y direction, and that the x-directed diffusivity is negligible. The equation is:

$$\frac{\partial}{\partial x}(bV_xC_{ij}) + \frac{\partial}{\partial z}[b(w_{ij}+V_z)C_{ji}] = \frac{\partial}{\partial z}\left[b\varepsilon_z\frac{\partial}{\partial z}(C_{ij})\right] \quad \textbf{(4-64)}$$

where: C_{ij} = local suspended sediment concentration (total mass of solids of ith-jth fraction per unit volume of fluid),
b = width of flow,
V_x and V_z = local longitudinal, x, and vertical, z, fluid velocities,
ε_z = vertical sediment diffusivity.

In gradually varied flows, the local vertical velocity V_z is considered to be insignificant when compared with the particle settling velocity for sand and gravel.

A numerical solution of (4-64) is formidable, and usually thankfully unnecessary. For reaches approximated by long-distance steps, the horizontal gradient term, $\frac{\partial}{\partial x}(bV_xC_{ij})$ becomes negligible, in which case integration of (4-64) yields the Rouse equation (Rouse, 1937):

$$\frac{C_{z_{ij}}}{C_{a_{ij}}} = \left(\frac{D-z}{z}\frac{a}{D-a}\right)^{\left(\frac{w_{ij}}{\kappa U_*}\right)} \quad \textbf{(4-65)}$$

where: $C_{z_{ij}}$ = concentration of ith-jth fraction at flow height z,
$C_{a_{ij}}$ = concentration of ith-jth fraction at flow height a,
a = height of moving-bed layer.

The reference concentration at the height of the moving-bed layer, $C_{a_{ij}}$ is calculated by assuming that grains in suspension have a concentration in the moving-bed layer predicted by the bedload equation. That concentration is defined as:

$$C_{a_{ij}} = \frac{i_{b_{ij}}}{U_{b_{ij}}ag} \quad \textbf{(4-66)}$$

where: $C_{a_{ij}}$ = concentration of ith-jth size-density fraction in moving-bed layer,
$U_{b_{ij}}$ = near-bed velocity of ith-jth size-density fraction,
a = thickness of moving bed layer,
g = gravitational acceleration.

An expression for $U_{b_{ij}}$ is:

$$U_{b_{ij}} = A(U_* - U_{*_{c_{ij}}}) \quad \textbf{(4-67)}$$

where suitable values of A range from 6.8 to 8.5. The moving-bed layer thickness a can be calculated using a relationship due to Einstein (1950):

$$a = 2D_{50} \quad \textbf{(4-68)}$$

where: a = grain saltation height,
D_{50} = mean grain diameter.

Equations (4-62) through (4-68) are incorporated in FORTRAN subroutine SUSP (Program 12) to calculate the suspended load of a steady, gradually varied unidirectional flow. The solution of the bed conservation equation is also included in Program 12. The reason for grouping these two solutions in the same subroutine is described in the next section.

Treatment of the Bed

As mentioned previously, once sediment transport begins, the bed texture and composition are modified. These modifications affect fluid flow and transport rates, thereby further modifying the bed. For this reason, the bed must be treated as a dynamic component of the system. This is accomplished by defining an *active layer* that consists of n well-mixed density fractions, each with its own size distribution. Each size class is represented by a median diameter D_{ij}. Particle exchange occurs between the active- and moving-bed layers during each timestep, after which the particle size-density distribution in the active layer is updated to allow for erosion or deposition of different size-density fractions. If net erosion occurs during the timestep, the active layer is replenished from the underlying parent bed material by an amount equal to the thickness of sediment eroded. If net deposition occurs, the base of the active layer moves up by an amount equal to the thickness of deposited material. The active layer thickness is defined as:

$$T_a = 2D_{50}\frac{\tau_o}{\tau_{c_{50}}} \qquad \textbf{(4-69)}$$

where: T_a = active layer thickness,

τ_o = effective temporal mean bed shear stress,

$\tau_{c_{50}}$ = critical shear stress necessary to entrain mean grain diameter.

Note that the active layer thickness increases with increasing excess shear stress. Its minimum thickness is the thickness of an armor layer of roughly two grain diameters.

Computation of the sediment mass exchange between the flow and the active layer, and consequent computation of erosion and deposition at each downstream site, is accomplished using the conservation of mass equation written for each size-density fraction. It is assumed that the timestep is sufficiently small so that fluid flow and sediment-transport rates may be considered constant over the timestep. The sediment continuity equation for a size-density interval expressed in terms of width-integrated sediment discharge is:

$$\sigma_j(1-p)\frac{\partial}{\partial t}(bz_{b_{ij}}) + \frac{1}{g}\frac{\partial}{\partial x}(bi_{b_{ij}}) + \frac{\partial}{\partial x}(S_{s_{ij}}) = 0 \qquad \textbf{(4-70)}$$

where: p = bed porosity

b = width of active bed, assumed to be equal to flow width,

$z_{b_{ij}}$ = bed elevation attributable to ith-jth bed fraction,

$i_{b_{ij}}$ = bedload (kg s^{-3}) transport rate of ith-jth fraction as defined in (4-61),

$S_{s_{ij}}$ = suspended load transport rate of ith-jth fraction as defined in (4-62) (kg s^{-1}).

Equation (4-70) is solved using a modified Preissman scheme (Lyn and Goodwin, 1987):

$$\Delta(bz_{b_{ij}})_t = \frac{1}{\sigma_j(1-p)}\{[\Phi(\Delta(i_{b_{ij}}+S_{s_{ij}})_{nd+1})]+[(1-\Phi)(\Delta(i_{b_{ij}}+S_{s_{ij}})_{nd})]\} \quad (4\text{-}71)$$

in which $\Delta(\text{variable})_{\text{subscript}} = (\text{variable})_{\text{subscript}} - (\text{variable})_{\text{subscript-1}}$, and Φ is a weighting factor between 0 and 1, and here set to 0.55.

These ideas are incorporated in the latter part of subroutine SUSP in Program 12 instead of a separate subroutine, because often more mass of a particular size can be transported by the flow than is present in the active layer. The transport rate for that size fraction must then be reduced. The process is iterative, and numerous calls among subroutines are slow in FORTRAN. Therefore we combine the two subroutines in SUSP to improve computation speed.

1-D ROUTING OF HETEROGENEOUS SIZE-DENSITY SEDIMENT OVER A MOVABLE BED: AN EXAMPLE

It is easy to lose sight of our goals, so a pause is in order. Our objective is to discuss the delivery of sediment from a source terrain to a basin. So far, we have derived a generic flow model that calculates local flow properties, such as cross-sectional mean velocity and water depth. We also have derived subroutines that predict the transportation and deposition of various size-density fractions in a unidirectional flow. Interaction of the transported material and the bed also is considered. We now need to assemble these components into an interacting whole. Such a model will have many applications, from predicting armoring below dams to sedimentary characteristics of fluvial strata in basins.

Here we discuss a 1-D numerical model of sediment routing within a relatively straight, nonbifurcating alluvial channel. The model simulates unsteady, nonuniform open-channel flow over an erodible, heterogeneous bed. The model calculates transport rates of each size-density fraction as a function of longitudinal position and time. As particles are eroded from or deposited on the bed, the channel hydraulic geometry may evolve or the bed may coarsen, thereby altering the flow hydraulics and fractional transport rates. The model is intended to simulate river evolution over geomorphic time intervals and therefore uses an uncoupled steady solution during each time step. In applying the model the reach of interest is subdivided into a number of longitudinal elements of varying width-averaged properties. During each time step, flow depths and velocities in each element are determined from the gradually varied flow equation using the standard step method (Program 4). The bedload and suspended-load transport rates of each size-density fraction are calculated with subroutines of Program 10 through Program 12. Interaction of the transported load and the bed is calculated by a bed continuity equation solved for each size density-fraction in an active layer (Program 12).

Solution of (4-1) through (4-71) proceeds according to the flow diagram of Figure 4-11. The reach of interest is discretized into a finite number of nodes, each Δx apart, at which hydraulic geometries and bed size-density distributions are known (Figure 4-12). At the start of each new timestep, the flow equations of the previous section (4-24) and (4-25) are solved using the standard step method of Henderson (1966), subject to a water-surface elevation at the downstream boundary node. Next, the skin-friction component of bed-shear stress (4-57) and (4-58) and a distribution of instantaneous bed shear stresses (4-59) are calculated at each node. After that, the

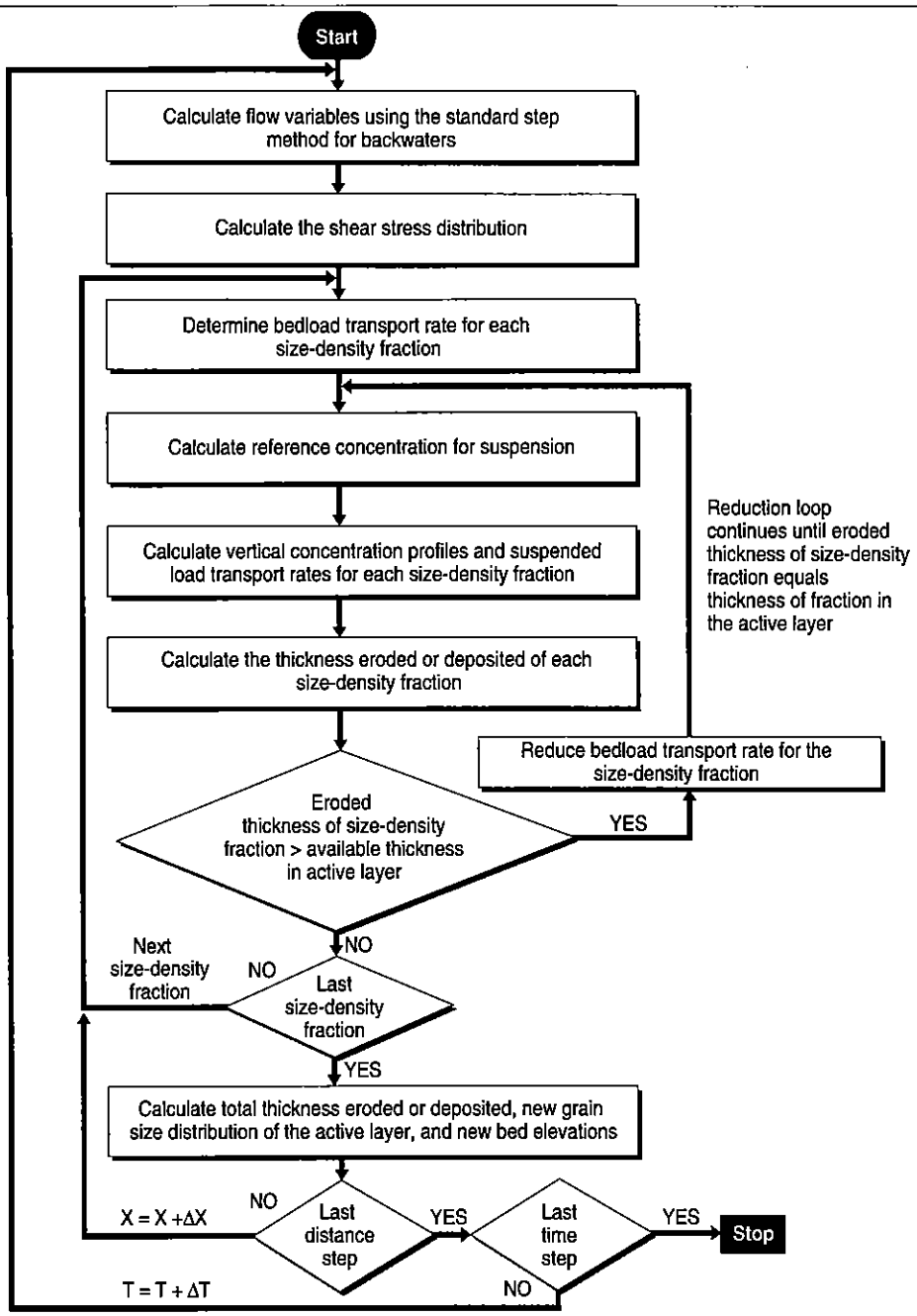

Figure 4-11 Flow chart of 1-D sediment-routing model.

critical shear stresses for suspension of each size-density fraction in the active layer at each node are calculated from (4-52), and the critical shear stresses for entrainment are determined using (4-41) through (4-44). Bedload transport rates of each fraction at each node are calculated with (4-61), which provides the reference concentrations necessary to calculate the suspended loads with (4-62).

The suspension profile is calculated from (4-65). Next, the bed continuity equation (4-70) is solved for each size-density fraction at each node, *nd*. If the theoretical transport rate of a certain size-density fraction exceeds the amount

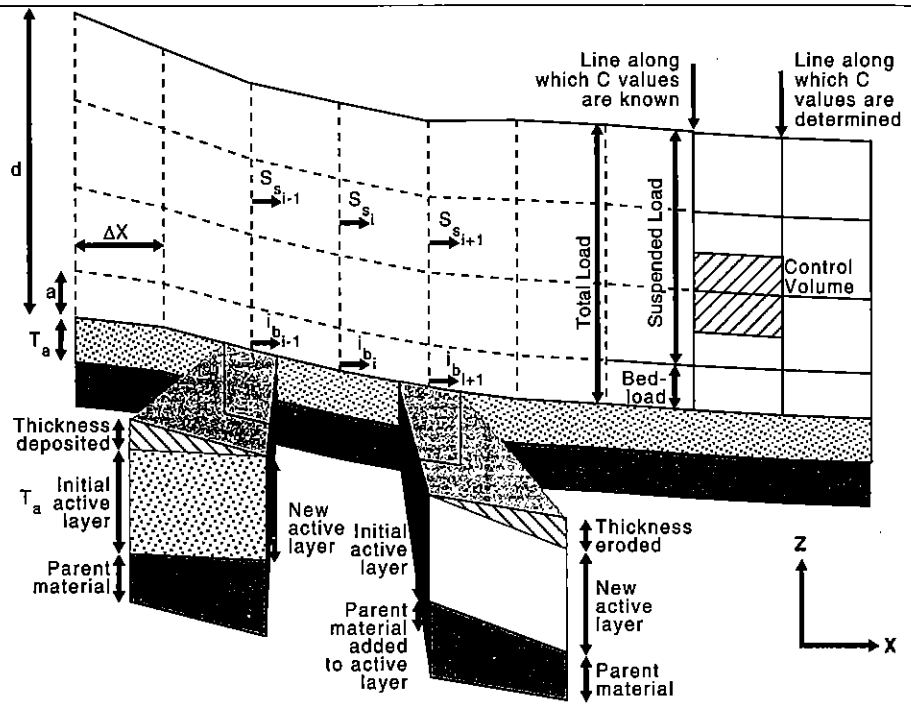

Figure 4-12 Schematic representation of grid used to calculate suspended load and treatment of bed after erosion and deposition. Effects of net erosion and aggradation on active layer are represented.

available in the active layer, the calculated bedload and suspended load transport rates of that size-density fraction are reduced until the amount eroded just equals the amount available. Finally, at each node, the size-density composition of the active layer and the bed elevation are recomputed, after which the computation proceeds to the next timestep.

Program 13 contains the main FORTRAN program which links the previously described subroutines together. It contains calls to numerous auxiliary subroutines, such as READRSTRT, which reads data if we want to restart calculations to extend a previous model run. It also contains WRFLDTA that writes output to certain files. These subroutines also are contained on the Programs diskette.

The two examples that follow demonstrate the use of the sediment-routing model and test its accuracy against flume and stream observations. A third example explores conditions under which a gold placer might form in an aggrading alluvial fan. Certain input parameters in the model are similar for all three example applications. First, the thickness of the moving bed layer is determined using the Einstein (1950) equation (4-68), and second, the active layer thickness is determined at the start of each numerical experiment with (4-69).

The active layer thickness is not allowed to vary dynamically during these experiments because at high flow strengths varying thicknesses make the model numerically unstable. However, at lower flow strengths, as in most of the experimental runs presented here, dynamically varying thicknesses of the active layer present no problems and lead to improved results. In the following discussion it should be kept in mind that all input parameters have either fixed values or values that vary only over a narrow range. In every case the actual flow and grain size values are used as input. No parameter has been adjusted to obtain a better fit.

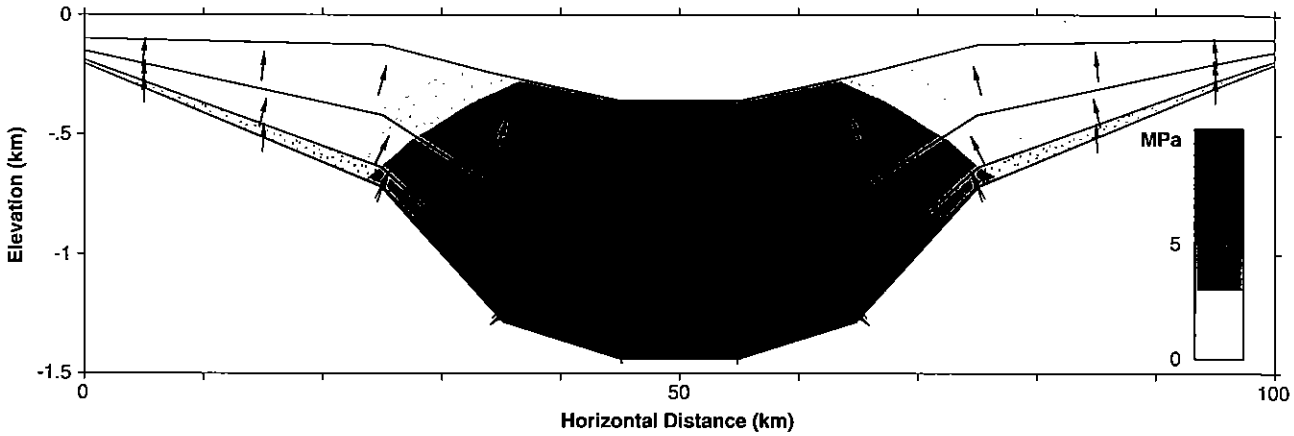

Plate 6-1

Experiment 6-1 representing failed-rift basin after five million years of elapsed time. Stippled pattern denotes sands, and shales are not stippled. Vertical section through basin shows main rift phase in which overpressures are shown with color contours in megapascals (MPa). Overpressures are defined as difference between hydrostatic pressure and actual fluid pressure. Variations in overpressures reflect rapid subsidence and accumulation of thick shales. Overpressures increase rapidly with depth because pore water cannot escape fast enough due to low permeabilities of shales. Arrows show directions of pore-water motions, which locally are downward in sands at base of sequence and upward in overlying shales. Velocities range too widely to be shown by differences in lengths of arrows. Compositions of beds provided as input to program in experiment are listed in Table 6-5. Sands at base of sequence were deposited in initial rift phase, whereas thick shales in central part of sequence were deposited in main rift phase. Vertical scale is 20 times horizontal scale.

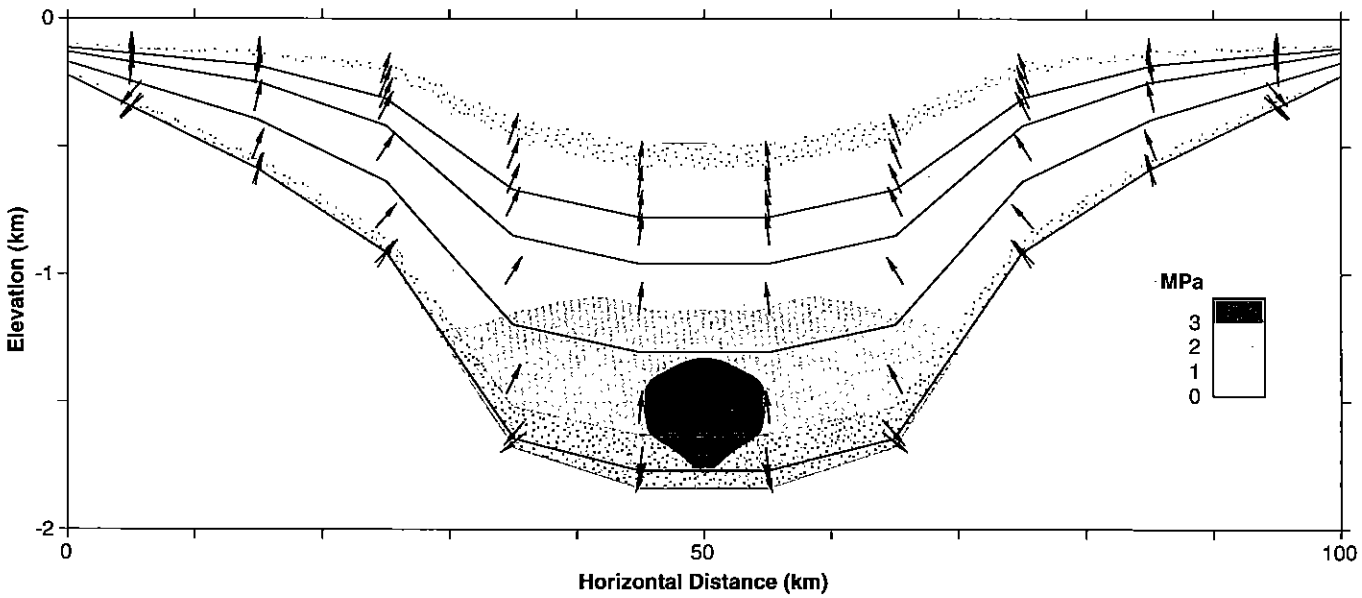

Plate 6-2

Experiment 6-1 representing failed-rift basin after 31 million years elapsed time, in sagging phase of rift. Color contours show overpressures. Overpressures are low throughout most of the basin, except in the lower central part of the basin, where they represent residual pressures from main rift phase. Stippled pattern denotes sands, and shales are not stippled. Mixed shales and sands in upper part of sequence were deposited during sagging phase of failed rift. Vertical exaggeration is 20 times. Arrows show direction of flow.

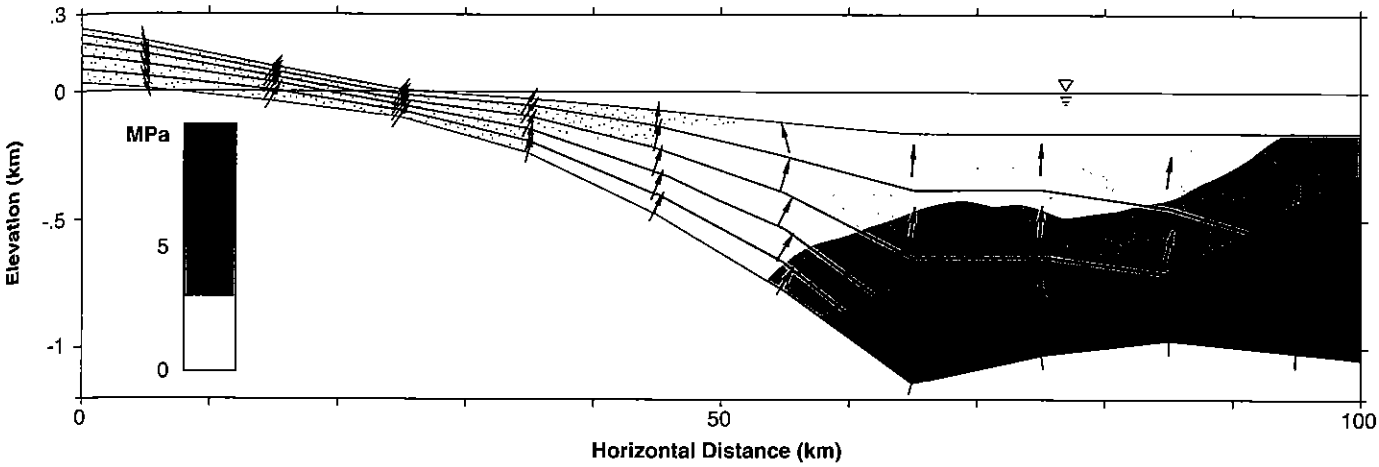

Plate 6-3

Experiment 6-2 representing prograding delta. Vertical section through basin is perpendicular to shoreline. Stippled pattern denotes sands, and shales are not stippled. Overpressures are shown with color contours in megapascals. Overpressures are defined as difference between hydrostatic pressure and actual fluid pressure. Overpressures increase rapidly within prodelta shales. Locations of maximum overpressures are related to progradation distance from river mouth and to variations in thickness of shales. Note topography induced flow in onshore area to left. Arrows show directions of pore-water motions. Velocities range too widely to be shown by differences in lengths of arrows. Flow directions are locally downward in recharge area, but are upward eleswhere. Shoreface sands prograde over former prodelta shales. Vertical scale is 20 times horizontal scale.

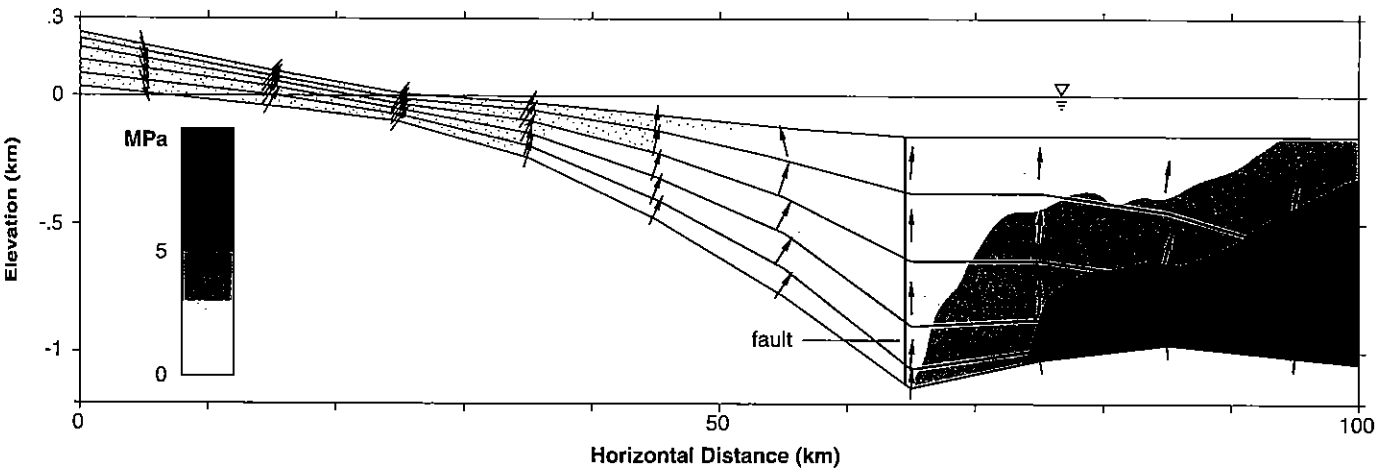

Plate 6-4

Experiment 6-2 representing prograding delta. Stippled pattern denotes sands, and shales are not stippled. Vertical section is similar to Plate 6-3, except that shales in single column shown by black bar to right of center of section, have been replaced by sand (which has high perrmeability), providing surrogate represention of vertical fault with high permeability. Color contours show that overpressures are strongly influenced by presence of fault, indicating rapid dewatering in its vicinity (compare with Plate 6-3).

Table 4-2 General hydraulic conditions for experiments used to test sediment-routing model

Data Source	Water Discharge (m^3/s)	Energy Slope	Manning's n ($m^{1/6}$)	Water Depth (m)
Little and Mayer (1972) Flume Experiment Run 3-4	0.016	0.0019	0.0153	0.066
Gold placer study (Vogel et al., 1992)	100	0.00001	0.04	4.75

Experiment 4-2: Flume Study of Little and Mayer

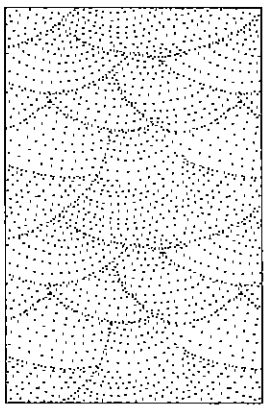

Little and Mayer (1972) investigated the effects of sediment gradation on channel armoring. A nonuniform bed of sand and gravel was placed in a flume 12.2 meters long, 0.6 meters wide, and 0.1 meters high. Clear water was passed over the bed to produce bed degradation and armoring. The eroded sediment was caught by screen separators at the downstream end of the flume, and at regular intervals was dried, weighed, and stored for later sieving. When the total transport rate was 1 percent of the initial transport rate and the armoring was thought complete, the flume was drained and the armor layer was sampled using molten beeswax as described by the authors. Here, we compare our sediment-routing model with Little and Mayer's experimental number run 3-4, for which the hydraulic conditions are listed in Table 4-2. The grain size distribution of the bed material (Table 4-3) from Little and Mayer's Table 3, is normalized so that the cumulative weight percentage equals 100 percent.

For numerical simulation modeling purposes the flume was divided into eight sections each of 1.525 meters length. The time step was 1 minute. In a series of sensitivity experiments, the time step was varied between 1 second and 10 hours. Model results were insensitive to time step if the time step was less than 5 minutes, and at time steps of up to1 hour model reproductions were still reasonably accurate. The active layer thickness, calculated from (4-69), was set to 0.002

Table 4-3 Grain size frequency distributions used in Experiment 4-2 and Experiment 4-4.

Little and Mayer Flume Experiment		Gold placer study of Vogel et al.: Quartz		Gold placer study of Vogel et al.: Gold	
Grain size interval (mm)	Percentage by weight	Grain size interval (mm)	Percentage by Weight	Grain size interval (mm)	Percentage by Weight
0.125-0.177	1.87	0.125-0.250	0.4	0.008-0.011	0.005
0.177-0.250	3.23	0.250-0.500	1.5	0.011-0.016	0.017
0.250-0.354	6.85	0.500-1	4.0	0.016-0.022	0.044
0.354-0.500	9.65	1-2	8.3	0.022-0.031	0.092
0.500-0.707	13.24	2-4	13.5	0.031-0.044	0.150
0.707-1.000	15.45	4-8	17.2	0.044-0.062	0.191
1.000-1.414	14.78	8-16	17.2	0.062-0.088	0.191
1.414-2.000	11.91	16-32	13.5	0.088-0.125	0.150
2.000-2.828	11.57	32-64	8.3	0.125-0.177	0.092
2.828-4.000	6.15	64-128	4.0	0.177-0.250	0.044
4.000-5.657	3.34	128-256	1.5	0.250-0.354	0.017
5.657-8.000	1.95	256-512	0.4	0.354-0.500	0.005

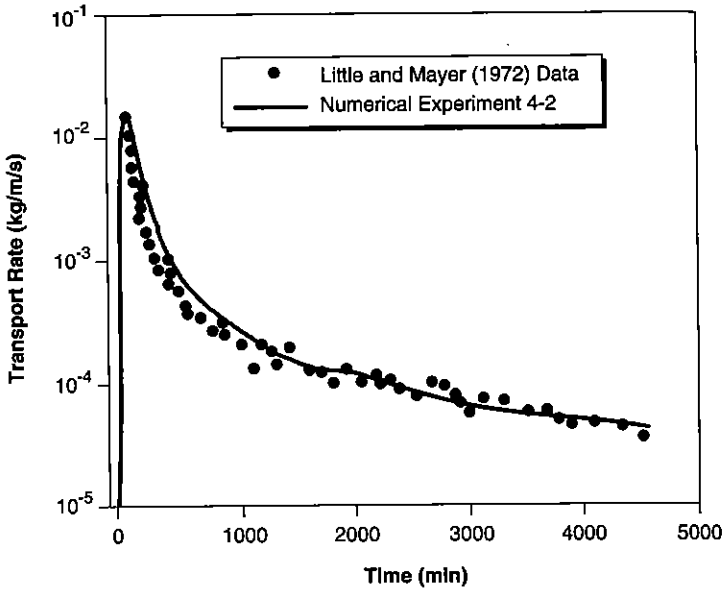

Figure 4-13
Plots of measured and computed sediment transport rate versus time for Little and Mayer's (1972) Experimental Run 3-4.

meters. The bed shear stress was not partitioned into form and skin components because bed forms were not present.

The computed and the measured total transport rates (Figure 4-13) show good agreement, in that the computed values are within a factor of 2 of the measured values at all times. Local fluctuations, the origins of which are unknown, cause only temporary divergence of the two curves. It may be, as Little and Mayer (1972) claim, that the turbulence spectrum produces random and intermittent movement of the bed particles. After 75.5 hours of flow, the size distributions of the original sediment, the bed-armor sediment, and the total eroded sediment (Figure 4-14) show that the numerically simulated armor layer is slightly finer

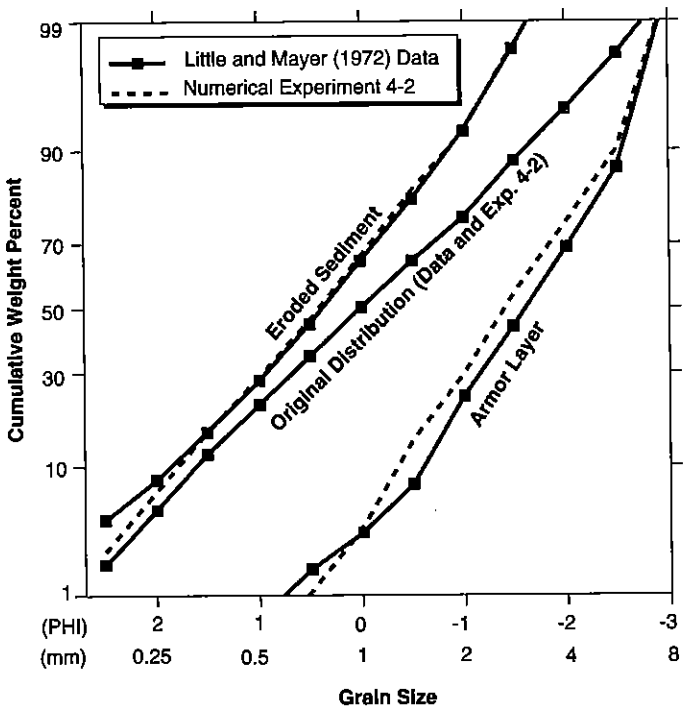

Figure 4-14
Cumulative log-log probability plot of measured and computed grain size distributions for Little and Mayer's (1972) Experimental Run 3-4 after 75.5 hours of flow.

than observed, although the difference in mean grain sizes is only 0.3 mm (2.7 mm versus 3 mm). The numerically simulated and physically observed grain-size distributions of the eroded sediment almost coincide.

Experiment 4-3: Field Study of the East Fork River, Wyoming

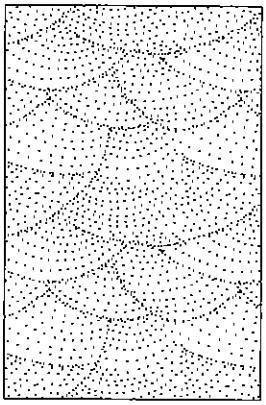

Sediment-transport and hydraulic data were collected by the U.S. Geological Survey (Leopold and Emmett 1976, Mahoney et al., 1976) from a bedload trap and flow gauges operated between 1973 and 1979, on the East Fork River, Wyoming (Figure 4-15). A 5-km reach upstream from the bedload trap provides an ideal test of a model's ability for numerical simulation of sediment transport under large-scale, nonuniform, unsteady flow conditions. For simulation purposes, the reach was divided into thirteen equally spaced segments between stations B-5 to B-17 (Figure 4-15). Segment end points define fourteen nodes, with node number 1 coincident with station B-17. At each node, a bed grain-size distribution was synthesized from twenty size fractions ranging between 0.0625 and 45.3 mm diameter, based on an interval average of the measured bed grain-size distributions. The simulated period extends from May 28, 1975, the day Leopold and Emmett measured the bed grain size distribution, to June 19, 1975, an arbitary termination date.

Two floods occurred in this period (Figure 4-16). The water discharge and flow depth at the downstream node (B-17), obtained from Leopold and Emmett's Table 1(1976), were assumed constant for a 24-hour period corresponding to the measurement day. Rectangular cross sections were assumed and widths at all nodes were kept constant in time. The bed shear stress was reduced to simulate the effect of bedforms on the effective bed shear stress. Sediment influx at upstream node B-5 was set to a value in equilibrium with the flow and the bed. Sediment influx from Muddy Creek (Figure 4-15), a tributary, was ignored because it consisted primarily of fines. The time step was 10 minutes and the active layer thickness, calculated from (4-69), was set to 0.005 meters.

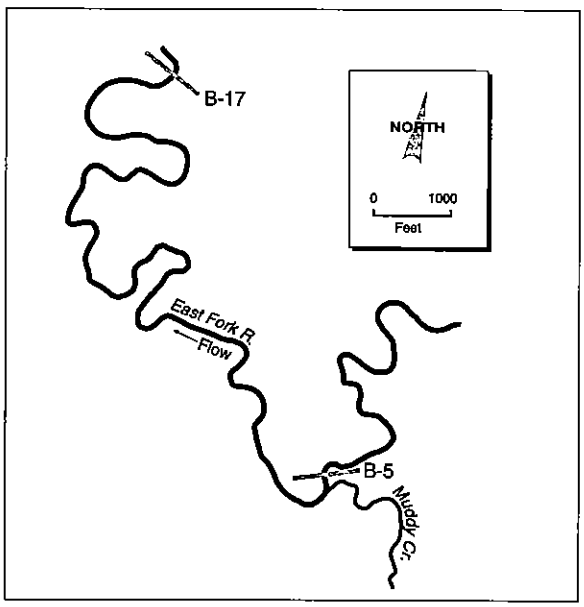

Figure 4-15 Sketch map of the study reach on East Fork River, Wyoming (after Mahoney et al., 1976). Data used in Experiment 4-3 were collected at station B-17. Station B-5 is start of modeled reach.

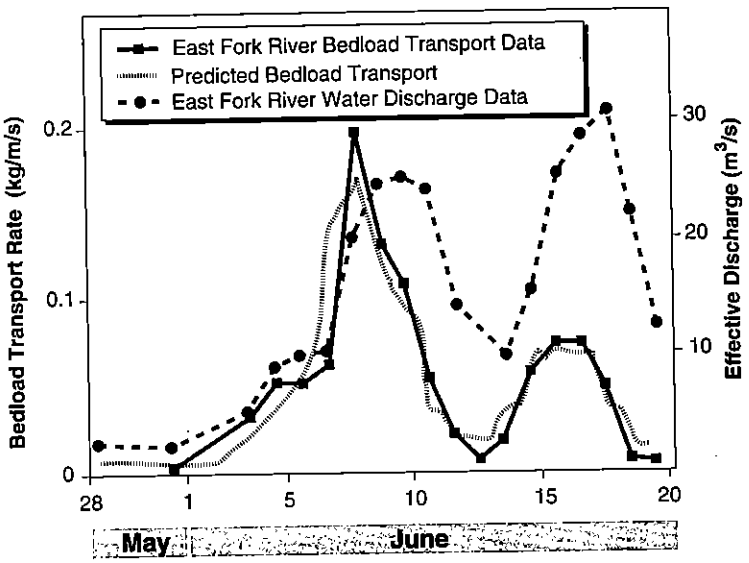

Figure 4-16
Plot of computed and measured bedload transport rates versus time, and measured effective water discharge (as defined by Leopold and Emmett, 1976) versus time at USGS facility, East Fork River, Wyoming, from May 28 to June 19, 1975.

The simulated bedload transport rates (dry weight of sediment transported through section B-17 per second per meter width) compare favorably with the rates measured by Leopold and Emmett (1976) as shown in Figure 4-16. The channel width used as a denominator for the measured values is 14.8 meters, which is the width of the bedload trap. The simulated bedload transport peaks match those of Leopold and Emmett in magnitude and date for both flood events. More importantly, the model accurately reproduces the grain-size distribution of the transported bedload (Figure 4-17). On June 2, 1975, before the first flood, the median size of particles in the bed was about 0.6 mm (Figure 4-17). By June 7,

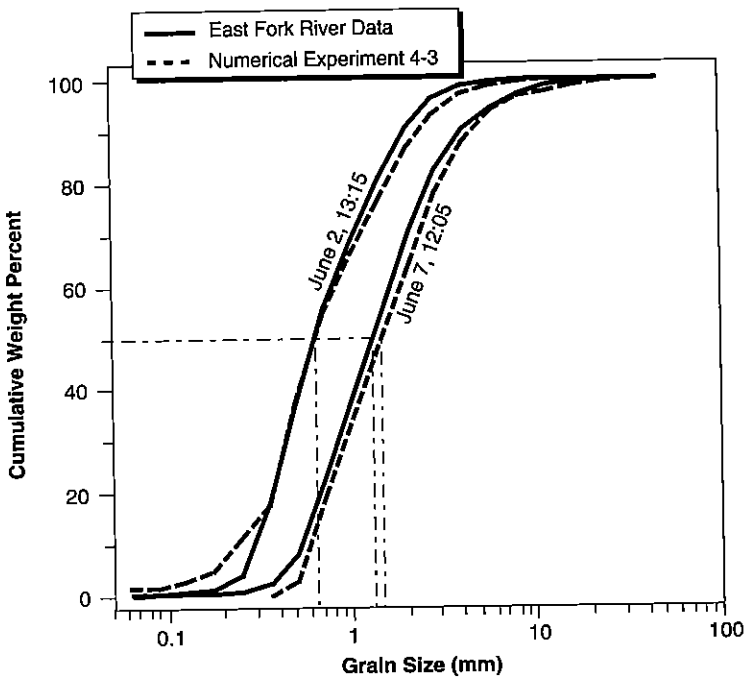

Figure 4-17
Cumulative frequency distribution of particle size for both observed and computed bedloads during two floods in East Fork River. Observed data from Leopold and Emmett (1976).

1975, at the height of the flood, both the measured and modeled grain-size distributions were coarser, such that the median was about 1.2 mm (Figure 4-17))

Curiously, the second flood, occurring between June 11 and June 19, 1975, produced lower bedload-transport rates than the first flood, although its peak water discharge was 19 percent higher (Figure 4-16). The reason is obvious when the modeled mean grain size of the bed material immediately upstream from the trap is compared for both flow events. At the start of the simulation run (May 28, 1975), nodes B-10 and B-11 had measured mean grain sizes of 0.9 and 0.5 mm, respectively, values which were finer than the average of the reach. By June 3, just before the first flood, this area of fine sediment had migrated downstream to segments B-13 and B-14, just upstream from the bedload trap at B-17. At the peak of the flood event (June 7), the readily entrainable fine sediment was transported to the bedload trap. By June 11, after the first flood, most segments were depleted in fine sediment, so that during the second flood, transport rates were lower. The first flood had partially armored the bed. Figure 4-17 compares the measured bedload grain-size distributions during the peak of the two flood events and confirms this interpretation, because during the second flood, the bedload grain size distribution was measurably coarser.

Experiment 4-4: Gold Placer Study

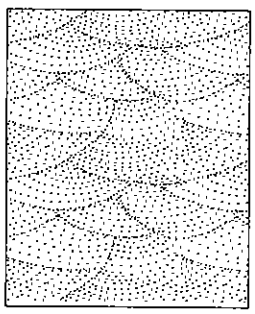

The sediment-routing model was developed to treat multiple grain densities, and is therefore useful for simulating heavy mineral placers. Probably the most famous heavy mineral placers in the world are the Witwatersrand paleoplacers of South Africa, the richest gold deposits in the world (Pretorius, 1976). In this example, we simulate the paleohydraulic conditions thought to have formed the 2.8-billion-year-old Ventersdorp Contact Reef, a paleoplacer of the Witwatersrand basin. It is thought to have accumulated as an aggrading alluvial fan.

The simulation consists of a 5-km long river with constant width of 100 meters and constant discharge of 100 m^3/s flowing over a flat surface with a slope of one in ten thousand into a standing body of water that was initially 4.75 meters

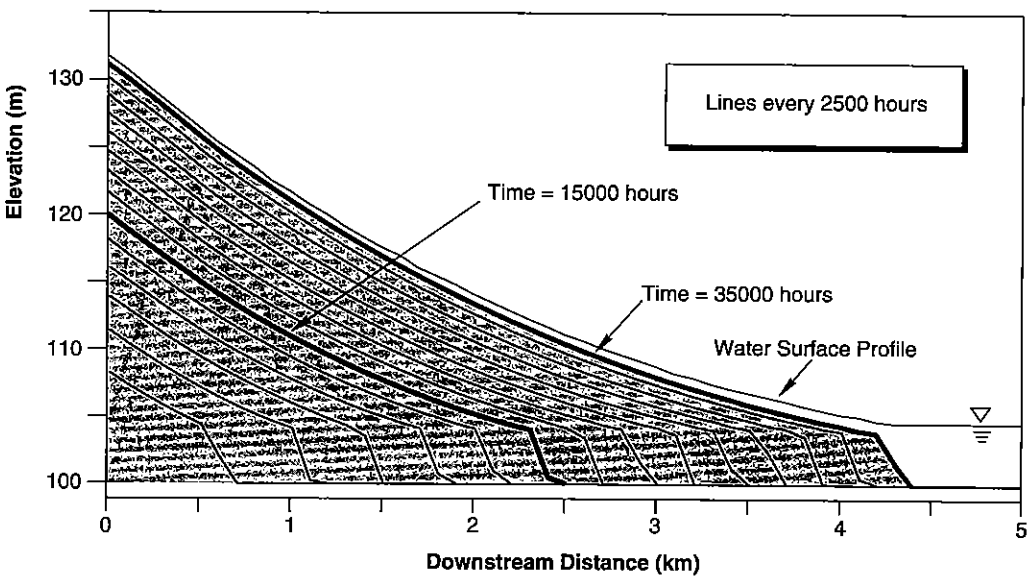

Figure 4-18 Longitudinal section through simulated gold-bearing alluvial fan in which time lines representing former bed surfaces are shown every 2500 hours of simulation time. Figure 4-19 plots gold concentrations versus distance downstream at 15000 hours.

deep. Sediment consisting of quartz and gold grains with constant phi-normal distributions entered at the river head. Grain size distributions supplied are summarized in Table 4-3. The sediment feed rates of the grain sizes, expressed in kg/m/s, are equal to the weight proportion of grains at the start of the experiment. For example, if a grain size makes up 1 percent of the bed, its feed rate is 0.01 kg/m/s. While the simulated slope and total weight percentage of gold are probably too high, we chose them to produce obvious temporal and longitudinal gold grade variations in the results.

Results show that the initial stream power of the river could not transport the mixture at the feed rate, causing sediment to accumulate at upstream nodes (Figure 4-18). Gradually, as more material was deposited, the bed slope increased and a concave profile alluviated and expanded. The gold was preferentially deposited at certain downstream locations, where conditions were favorable for placer genesis (Figure 4-19).

Ideal placer locations are a function of many factors, the main two being heavy mineral grain size and bed shear stress, the latter in turn a function of bed slope and downstream distance. In the experiment, after 1.75 years (Figure 4-19), the first 1200 meters of the stream show, on average, a bed enriched in relatively coarse gold, with concentrations steadily decreasing with distance; the 1500 meters that follow are depleted in gold. Beyond 2700 meters downstream the river bed returns to its original concentration because the bed has not yet been altered due to deposition or erosion. Relatively fine-grained gold, also with an original weight percentage of 0.158 percent in the bed and feed, was depleted over the first 500 meters. Over the next 2200 meters its average weight percentage steadily increased, eventually peaking at 2500 meters downstream. The intermediate-size gold grains, with an original weight percentage of 0.682 in the bed and feed, yield a bell-shaped concentration curve, with a peak at 1500 meters downstream.

The origin of these distributions may be explained as follows: Relatively coarse gold is entrained only at high shear stresses, and once it enters the river system is not transported very far, thus accounting for enrichment at the stream head. Between 1200 and 2700 meters downstream, the concentration remained low because the original bed, where relatively coarser gold made up 0.158 per-

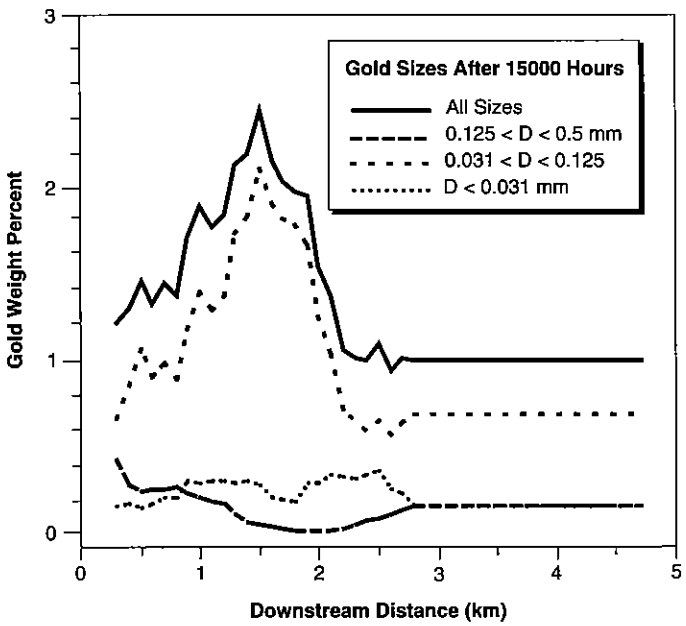

Figure 4-19
Plot of proportion of gold, expressed as gold weight percentage, versus distance downstream after 15000 simulated hours in Experiment 4-4. Gold weight percent is expressed as moving average (n=5). Gold grain-size distribution was divided into three intervals: relatively coarse-grained, between 0.125 and 0.5 mm; intermediately-sized, between 0.031 and 0.125 mm; and relatively fine-grained, smaller than 0.031 mm. Coarser- and finer-grained gold represent 0.158 percent of both feed and bed at start of experiment, while intermediate-sized gold represents 0.682 percent.

cent, was buried by sediment impoverished in coarse gold. Relatively fine gold, on the other hand, was readily entrained under the stream shear stresses, and occurs over the length of the stream. The fact that bed weight percentage of gold is greater than that of the feed seems to indicate that gold is more difficult to transport than quartz. Its preferential deposition at 2500 meters seems to indicate that fine gold is transported reasonably well by the river system and was deposited when the gentle slope at 2700 meters was reached. The intermediate-size gold shows an intermediate behavior. At the head of the stream, the flow could entrain it and transport it downstream. At about 1500 meters downstream, the bed-shear stress dropped below a value at which, on average, the medium-grained gold could be entrained and transported, resulting in deposition of gold. While still partially entrainable after 1500 meters, most of the medium-grained gold was not entrained and transported past that point.

A SIMPLER FORMULATION: YANG'S BED-LOAD FORMULA

For some applications, it may not be necessary to know the detailed bed and sediment-load textures. In these cases, we can use a transport model that predicts bed-material discharge given only the median size of grains in the bed and a few flow characteristics. Bed-material discharge is defined as the discharge of all particles derived from and readily exchanged with the bed. Extensive summaries of bed-material discharge formulas as provided by various authors (Alonso et al., 1981; ASCE, 1976; Yang and Wan, 1991; Stevens and Yang, 1989) and compare measured and computed results. Our conclusion is that Yang's formulas are reasonably accurate, simple, and cover the range of grain sizes interesting to geologists.

Yang derived two equations that predict the concentration of the bed-material discharge, one for sand-bed streams and one for gravel-bed streams. Their derivations are based on dimensional analysis and the concept of unit stream power, VS, a measure of the rate of potential energy dissipated per unit weight of water, where V is velocity and S is stream slope. Coefficients for both equations were obtained by multiple regression. For the sand-bed equation, 463 sets of laboratory data on flow and sediment parameters cover a range of median sieve diameters from 0.015 to 1.71 mm. For the gravel-bed equation, 166 sets of laboratory data cover a range from 2.46 to 7.01 mm. The two equations are of the same form and differ only in coefficients A through H:

$$\log C = A - B\log\left(\frac{wD_{50}}{\nu}\right) - E\log\left(\frac{U_*}{w}\right) + \left[F - G\log\frac{wD_{50}}{\nu} - H\log\frac{U_*}{w}\right]\log\left(\frac{VS}{w} - \frac{V_{cr}S}{w}\right) \quad (4\text{-}72)$$

where: C = concentration of bed-material discharge in parts per million by weight,

A, B, E, F, G, H = regression coefficients for sand or gravel given in Table 4-4,

w = fall velocity of the median size in m/s,

D_{50} = median diameter of grains in bed in m,

ν = kinematic viscosity in m^2/s,

U = shear velocity in m/s,

V = average flow velocity in m/s,

S = energy slope,

V_{cr} = dimensionless critical velocity at incipient motion, expressed as:

Table 4-4 Coefficients for Yang's bed-material equations (Yang, 1973).

Bed	A	B	E	F	G	H
Sand	5.435	0.286	0.457	1.799	0.409	0.314
Gravel	6.681	0.633	4.816	2.784	0.305	0.282

$$\frac{V_{cr}}{w} = \left(\frac{2.5}{\log\left(\frac{U_* D_{50}}{\nu}\right) - 0.06} \right) + 0.66 \quad \text{for } 1.2 < \left(\frac{U_* D_{50}}{\nu}\right) < 70 \tag{4-73}$$

or:

$$\frac{V_{cr}}{w} = 2.05 \qquad \text{for } 70 \leq \left(\frac{U_* D_{50}}{\nu}\right) \tag{4-74}$$

Equations (4-72) through (4-74) have been coded in the FORTRAN subroutine in Program 14. The required fall velocities can be obtained from the subroutine in Program 7, and shear velocities, average flow velocities, and energy slopes can be obtained from the gradually varied flow model in Program 4.